Quasinormal Modes of Gubser-Rocha Holomatter

Aretz, Joost

Quasinormal Modes of Gubser-Rocha Holomatter

THESIS

submitted in partial fulfillment of the
requirements for the degree of

MASTER OF SCIENCE
in
RESEARCH IN PHYSICS: CASIMIR

Author :	Joost Aretz
Student ID :	1802941
Supervisor :	Prof. Dr. Jan Zaanen
	Nicolas Chagnet
2^{nd} corrector :	Prof. Dr. Koenraad Schalm

Leiden, The Netherlands, July 4, 2022

Quasinormal Modes of Gubser-Rocha Holomatter

Joost Aretz

Instituut-Lorentz, Leiden University
P.O. Box 9500, 2300 RA Leiden, The Netherlands

July 4, 2022

Abstract

Motivated by the search for a holographic generalisation of the strange metal phase, this thesis investigates the quasinormal modes of the AdS_4 Gubser-Rocha black hole. Gauge-invariant modes of the black hole perturbations are derived which simplify computation enormously. Using relativistic hydrodynamics we associate the quasinormal modes with conserved quantities of a charged fluid. Low temperature discrepancies with the hydrodynamic predictions for the temperature dependence of the modes are observed in the sector longitudinal to the perturbations. The suspected cause of the discrepancy lies in the need for non-trivial sourcing of the scalar field. The method to correctly source the scalar field is discussed.

Contents

Version of July 4, 2022– Created July 4, 2022 - 20:01

Chapter 1

The AdS/CFT correspondence

The AdS/CFT correspondence is a powerful mathematical tool which allows us to draw parallels between gravitational- and quantum field- theories. This insight which was derived from string theory has opened new inroads for researching the relation between general relativity and quantum mechanics. Recently the correspondence has started to cross-over to the domains of condensed matter physics as well. This exciting development allows for a radically new description of transport through materials in the absence of (quasi-)particles. This thesis sets out to study the quasinormal modes of the Gubser-Rocha black hole in AdS_4 motivated by the AdS/CFT correspondence's application to one of the biggest unsolved problemss in condensed matter physics; The strange metal.

The reader will first be introduced to the essentials in three parts before moving to methods, results and discussion: Chapter 1 will introduce AdS/CFT. Chapter 2 will motivate the connection to condensed matter, while Chapter 3 will introduce the required background knowledge of hydrodynamics.

1.1 The essence of AdS/CFT

The AdS/CFT in it's original form by Maldacena [1] conjectured the duality between Anti-de-Sitter gravitational theories in d+2 dimensions and quantum conformal field theories in d+1 dimensions. All the information of the gravitational theory is stored in one less dimension, hence the name holographic duality. In our case the CFT will be viewed as a condensed matter system we wish to study the transport properties of. The gravi-

tational theory will be the tool we use to do computations and the holographic duality allows one to translate the results from the gravitational calculation to the CFT properties.

The essence of the duality lies in its ”weak-strong”-nature. The strong refers to the CFT coupling while the weak refers to gravitational theory being of the classical (not quantum) type and thus computable. Calling the CFT ”strong” is a simplification of the original conjecture where the CFT is ”in the large N limit for inifinite 't Hooft coupling”. Large N here refers to the number of local degrees of freedom. It is unclear what this large N limit would physically represent in system, but it is a requirement for the gravitational theory to be classical in nature and thus computable. There are many more intersting questions to ask regarding the meaning of the large N limit and infinite van 't Hooft coupling, but we will take it to mean the CFT is strongly interacting and quantum critical. For an argument the reader is referred to introductory books of applying holography to condensed matter [2, 3]. The crucial point is that a strongly interacting quantum critical CFT cannot simply be quantized through standard techniques and is thus difficult to study directly. We will get back to this in Chapter 2. The duality provides a method to avoid this problem by studying the gravitational dual and using the holographic duality to translate.
Shortly after the discovery of the holographic duality the GKPW-dictionary was established simultaneously by Witten and Gubser, Polyakov and Klein. [4, 5] The dictionary eq. 1.1 translates between the boundary CFT (Left) and the bulk gravitational theory (Right).

$$\left\langle e^{\int d^{d+1}x J(x)O(x)} \right\rangle_{CFT} = \int D\phi e^{iS_{bulk}(\phi(x,r))|_{\phi(x,r=\infty)=J(x)}} \tag{1.1}$$

The dictionary can be viewed as analogous in spirit to the Fourier transform for the particle-wave duality. It allows us to translate between representations. From eq. 1.1 we see that sources J of operator O in the CFT are related to the boundary behaviour ($r \to \infty$) of the bulk field ϕ which we call dual to O. The table below shows some entries of the dictionary. The take-home message of this section is that the near-boundary behaviour of the bulk fields sets both the source and the vacuum expectation value the dual CFT operators. In section 4.3 we will use this to probe the CFT response through bulk calculations.

AdS bulk field	**CFT boundary operator**
metric $g_{\mu\nu}$	energy momentum tensor $T_{\mu\nu}$
gauge field A_μ	current J_μ
scalar field ϕ	scalar operator O

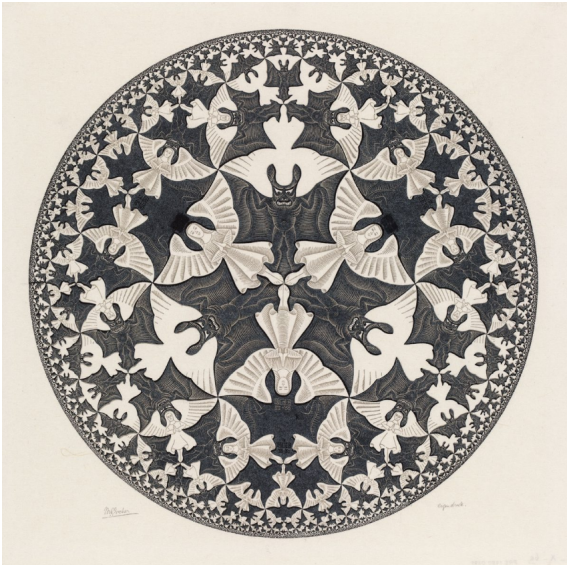

Figure 1.1: *Circle Limit IV, M.C. Escher. This figure demonstrates the isometry of AdS space. As you move outward radially the scale decreases, but the geometry remains unchanged.*

1.2 RG GR

This section will explain the meaning behind the extra dimension of the gravitational theory as well as introduce the underlying isometry which lies at the heart of the duality. The simplest AdS spacetime imaginable is

$$ds^2 = \frac{1}{r^2}(-dt^2 + dx^2 + dy^2 + dr^2), \tag{1.2}$$

From this metric we can directly observe an isometry. The metric tensor is invariant under scale transformations $x^\mu \to \Lambda x^\mu$. The result of the scale transformation is identical to varying the radial coordinate r. This isometry is captured by figure 1.1 where moving outward from the centre of the picture is akin to increasing the r coordinate and scaling down the pattern. It turns out that such isometries of the bulk spacetime can be linked directly through the GKPW dictionary to the symmetries of the boundary CFT.

This bulk isometry under scale transformation and the form of the AdS metric 1.2 hints at the meaning of radial coordinate r. The radial coordinate is precisely the extra dimension absent in the boundary CFT and it encodes for the energy scale of the CFT, similar to how to encodes scale transformation in the bulk. Thus the radial coordinate is responsible for a

Version of July 4, 2022– Created July 4, 2022 - 20:01

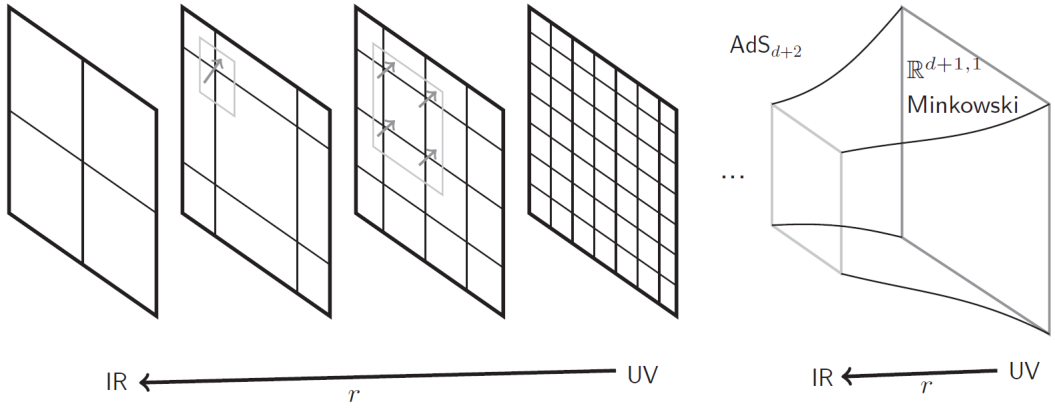

Figure 1.2: *Figure demonstrating the GR=RG principle at work.*

renormalization flow of the boundary CFT. Figure 1.2 illustrates this phenomenon. As we move along the radial coordinate the field theory described by the boundary becomes increasingly coarse-grained.

1.3 Finite Temperature

The original AdS/CFT duality was conjectured at zero temperature, but it was quickly realised that there is a way to bring the boundary CFT to finite temperature. A logical first place to look would be the only objects in GR which have a temperature associated with them; Black holes. Indeed, it was found that placing a black hole in the deep IR (the left side of 1.2) raises the temperature of the boundary CFT. It is the Hawking temperature, proportional to the black hole horizon area, which sets the CFT temperature. In fact as one might suspect from knowledge of black holes from general relativity the black hole introduces an IR cut-off and long wavelength physics is Debye screened. The information of the theory beyond the black hole horizon is in this regard hidden, similar to how black holes hide information beyond their horizon in typical general relativity.

We can identify the temperature of a typical black hole metric by the following procedure. First, we Wick rotate ($t \to i\tau$) a general black hole metric to obtain

$$ds^2 = \frac{1}{r^2}(f(r)d\tau^2 + \frac{dr^2}{f(r)} + dx^i dx^i). \tag{1.3}$$

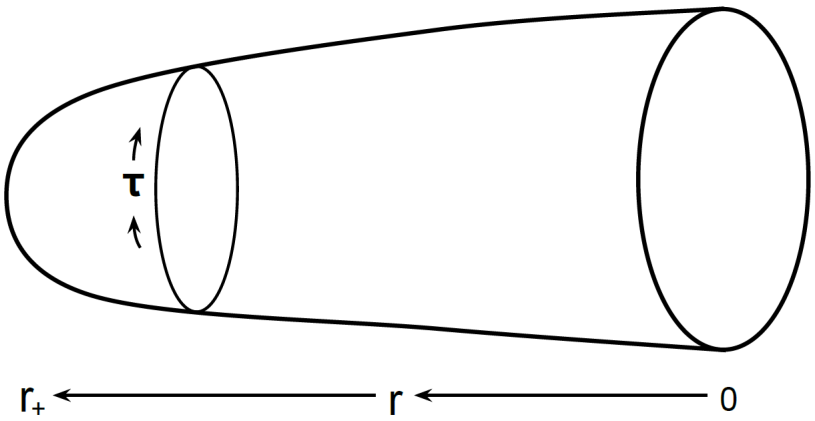

Figure 1.3: *Cigar geometry aka the euclidean time circle. Figure source:[2]*

For black holes the emblackening factor $f(r)$ becomes 0 at the horizon and switches sign. If we expand the metric near the horizon and transform coordinates to $\rho^2 = \alpha(r - r_+)$ and $\phi = \beta\tau$ the metric becomes of the form:

$$ds^2 = d\rho^2 + \rho^2 d\phi^2 + \frac{dx_i^2}{r_+^2}. \tag{1.4}$$

The geometry of the $\{\rho, \phi\}$-part of the metric is illustrated in figure 1.3. There then appears to be a conical singularity at the horizon as any value for ϕ collapses unto a point. The $\{\rho, \phi\}$-part of the metric in equation 1.4 at the horizon ($\rho \to 0$) is simply flat space at the origin in polar coordinates of the polar coordinate system. To regularise this we must identify $\phi = \phi + 2\pi$. Working back we then identify a periodicity in τ. This is analogous to equilibrium systems in quantum mechanics where the temperature is associated with the periodicity of the euclidean time circle $\tau = \tau + 1/T$. In the next section we will see how temperature sets the periodicity of the euclidean time in quantum mechanical systems.

$$T = \frac{|f'(r_+)|}{4\pi}. \tag{1.5}$$

1.4 Quantum criticality

It is generally understood that the Conformal field theory duals in the AdS/CFT correspondence are quantum critical. This section aims to introduce the concept of quantum criticality. A detailed introduction to the

subject can be found in [6]. This section will only discuss general details of interest to understanding holography and it's connection to strange metals. Quantum criticality is the quantum incarnation of criticality known from regular statistical mechanics. In regular statistical mechanics the critical point is associated with a phase transition and the onset of scale invariance. The spatial correlation function diverges. Around the critical point in the phase diagram the physics of the system is governed by critical exponents. The beauty of this discovery lies in universality which implies that the phase transition of a magnet from order to disorder can be governed by the same dimensionless critical exponents as the transition of water to steam.

Quantum critical systems are very similar in the sense that they must be fine-tuned to the critical point and the behaviour around this quantum critical point (QCP) is governed by critical exponents. The quantum critical point lies at zero temperature which means it is unstable and practically inaccessible; Any (quantum) fluctuation brings the system away from the QCP. Another important feature is that the scale invariance is promoted to conformal invariance; Invariance under all locally angle preserving transformations. Note that this is the symmetry which defines conformal field theories. Quantum criticality does introduce another scaling exponent; z, the dynamical critical exponent. z describes how the euclidean temporal dimension and the spatial dimensions in some cases (when $z \neq 1$) can no longer be treated on the same footing. Another typical feature of the quantum critical state which can be observed in experiment is the absence of scale in response function:

$$G(\omega, k) \sim \frac{1}{k^2 - \omega^2}. \tag{1.6}$$

Response functions of this form are called branch-cuts as they have branch-cut divergences instead of isolated poles. This is in stark contrast to typical response functions of particle physics which typically contain a self-energy term. An example of self-energy is the renormalized electron masses in Fermi-liquid theory. Such mass terms introduce intrinsic scale in the response functions and are incompatible with the scale invariance of the critical state.

1.4.1 Finite temperature quantum criticality

First we introduce an important concept in modern statistical quantum physics. The Wick rotation used in the previous section is a trick also commonly used in quantum statistical physics. The Wick rotation can be used to map quantum problems onto well known statistical physics problems. This can be seen by observing the form of a general quantum partition sum in the path integral formalism:

$$Z_\hbar = \int Dq e^{iS_{\text{path}}/\hbar}, \tag{1.7}$$

$$S_{\text{path}} = \int dt \mathcal{L}_{\text{path}}, \tag{1.8}$$

Here the integral is over all possible paths of evolution through phase space the system may take. After a Wick rotation $t \to i\tau$ the partition sum turns simply into the well known partition sum used in statistical mechanics. The exponent in the partition sum turns into the typical statistical probability $e^{-S_e/\hbar}$. It was discovered by Kubo that viewing the euclidean time τ as defined on a circle of radius $R = \hbar/k_B\tau$ (like fig. 1.3) one can use this to compute finite temperature equilibrium physics. This works perfectly when the action consists of bosonic operators. When the action contains fermionic operators life becomes more difficult as their anti-commutation relations introduces signs into the action. The result is that in some configurations the probability becomes larger than one. This is known as the fermion sign problem. Chapter 2 will refer back to this point.

The result for the finite temperature physics near quantum criticality is that our temperature has now introduced a scale in the system; the time circle radius. The result is that at finite temperature response functions give in to energy-temperature scaling:

$$G(\omega, k) = \frac{1}{T^\Delta} F(\frac{\hbar\omega}{k_B T}). \tag{1.9}$$

Here F is some response function and Δ is the anomalous scaling dimension.

Finally a property of the quantum critical system is the planckian timescale. One can infer that these systems at finite temperature near criticality should know of only one timescale: the timescale associated with the time circle

radius. Dissipative physics in general at long length and time scales is set by a characteristic timescale associated with the diffusion of the system. In these finite temperature near critical systems there is only one characteristic timescale; The Planckian timescale. Thus dissipation in systems near criticality must be set by the Planckian time $\tau_\hbar$. This time is incredibly short and is seen as a lower bound on characteristic timescales of dissipation processes. Interestingly, Planckian dissipation was observed in the critical quark gluon plasma [7]. Estimates from conventional quantum field theory techniques were orders of magnitude off. In models of holographic matter the Planckian time arises naturally in the dual critical CFT.

1.5 Holographic models

The details of the boundary CFT are dependant on the choice of bulk gravitational theory. For our intents the model of choice is a model containing gravity, electrodynamics and a scalar field. This class of models is known as Eistein-Maxwell-Dilaton (EMD) models. Equation 1.11 displays a typical Bulk action of such a model. Their great advantage over the well studied and comparatively simple Einstein-Maxwell models (eq. 1.10) is that they have zero entropy at zero temperature.

$$S_{EM} = \frac{1}{2\kappa^2}\int d^4x\sqrt{-g}[R - F^{\mu\nu}F_{\mu\nu} - 2\Lambda] \tag{1.10}$$

$$S_{EMD} = \frac{1}{2\kappa^2}\int d^4x\sqrt{-g}[R - Z(\Phi)F^{\mu\nu}F_{\mu\nu} - \frac{3}{2}(\partial_\mu\Phi)^2 + V(\Phi)] \tag{1.11}$$

For the EM-action we study the Reissner-Nordström solution detailed in A. For our EMD model we study the Gubser-Rocha black hole we derive in 4.1 Gouteraux Kiritsis [8] discovered that holographic theories at finite low temperature have general IR behaviour set by:

$$ds^2 = \frac{1}{r^2}\left(-\frac{dt^2}{r^{2d(z-1)/(d-\theta)}} + r^{2\theta/(d-\theta)}dr^2 + d\overrightarrow{x}^2\right). \tag{1.12}$$

Where z is the dynamical critical exponent we learnt of in the previous section. θ is another anomalous critical exponent called the hyperscaling violation, which describes the entropy scaling of the system. In the Fermi liquid entropy scaling is set by the presence of the Fermi surface which has spatial dimension $d-1$ and hence Fermi liquids have $\theta = d-1$. From [2] we learn that the entropy scaling behaviour of holographic theories is

then set in general by:

$$S \sim T^{\frac{d-\theta}{z}}. \tag{1.13}$$

In the Fermi liquid $z = 1$ and the entropy is Sommerfeld $S \sim T$. For Einstein-Maxwell models one arrives at the Reissner Nordström black hole which is characterised by $z \to \infty$. The result is that the entropy does not vary with temperature. For our EMD model we study the Gubser Rocha black hole named after its inventors [9]. The Gubser Rocha black hole is characterised by $z \to \infty$ and $\theta \to -\infty$ such that the exponent in equation 1.13 becomes precisely 1, which means the entropy of the GR black hole is Sommerfeld like that of the Fermi liquid and the strange metal.

Version of July 4, 2022– Created July 4, 2022 - 20:01

Chapter 2

Relevance to Condensed Matter

The popularity of holography in recent years is owed in part to the condensed matter community. This is due to the fact that holographic models provide a machinery by which one can use gravitational computations with matter fields to study strongly interacting field theories. Conventional perturbative techniques fail for such strongly interacting electron systems. This is largely due to the Fermion sign problem which was teased in the previous chapter.

A specific example of system in nature which is expected to be governed by strongly interacting electron interactions is the strange metal phase. This thesis sets out to investigate the hydrodynamic behaviour of a holographic model of particular interest in the quest for a holographic description of strange metal behaviour; The homogeneous Einstein-Maxwell-Dilaton model. This chapter will motivate the application by sketching the basic problems conventional approaches encounter in critical matter and discuss indications that holography might offer an alternative description.

2.1 Semi-Classical Matter

To understand the need for a new description of strongly interacting critical matter one must first obtain a view of the current paradigm of quantum mechanics. In this section the standard operating procedure for a condensed matter quantum mechanic will be described.

When physicists set out to model a system the first order of business is to establish an action principle of the system. The action contains all of the

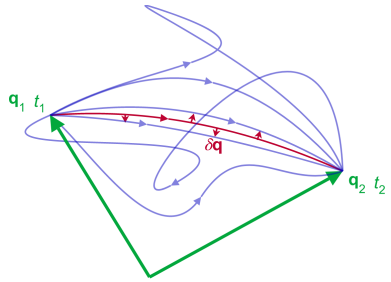

Figure 2.1: *Possible evolutions of a system from state 1 to state 2 in phase space. Red highlights the classical path of least action while other paths are blue. All imaginable paths from 1 to 2 are allowed but the classical path has the highest likelihood. Source:[10]*

ingredients (particles and interactions) of a theory and how they interact with each other. To describe the system we then choose some initial state of the system. In classical physics one then uses the principle of least action to predict the path in phase space along which the system will evolve. Figure 2.1 illustrates such a path of least action in red. In quantum mechanics all imaginable paths through phase space are allowed evolutions of the system, but the probability of a path being taken is weighted by the action of the path equation 2.1. The classical path is still unique in that it is the path of highest probability. This is the starting point of any description by Feynman's path integral formulation of quantum mechanics.

$$P(\text{path}_\text{j}) = \frac{1}{Z} e^{-\frac{iS_j}{\hbar}} \tag{2.1}$$

In equation 2.1 Z is the quantum partition sum we have discussed previously in section 1.4. Ubiquitous in the semi-classical approaches to quantum mechanics is that there is one classical state or "path" dominating over the other states. Take for example equation 2.2 to describe a general state of the system. In semi-classics there is one "classical" $|\psi_{cl}\rangle$ (the groundstate or vacuum) such that its probability amplitude is much larger than the other states $a_{cl} >> a_i$.

$$|\Psi\rangle = \sum_i^N a_i |\psi_i\rangle \tag{2.2}$$

This makes life easier as it allows a physicist to use his or her favorite tools; perturbative techniques. One uses the classical state as a zeroth order approximation and then adds quantum corrections perturbatively. This is in simplified terms the essence the current paradigm from the descriptions of

the Fermi-liquid to BCS theory of superconductivity to the application of the standard model on particle collisions in CERN experiments. The methods critically depend on being able to identify one state which dominates over the others.

2.2 Strong interactions & Long range entanglement

These methods start to fail in models where interactions are strong or where there is many-body entanglement. The problems are especially large in fermionic systems. Strong fermion-fermion interactions lead to states which are long-range many body entangled. Many body entanglement here refers to no one state from eq. 2.2 dominating. The strength of the interaction makes it difficult to identify a suitable small parameter with which to do a perturbation expansion. What's worse, the many body entanglement makes it so that it is unclear which "classical" state one should choose to expand around.

The origin of the problem can be traced back to a simple lesson all physicists should be familiar with. Take a system of N qubits which can occupy the state 0 or 1. The wavefunction of a state takes the form:

$$|\Psi\rangle = |\psi_1\rangle \otimes |\psi_2\rangle \otimes |\psi_3\rangle \otimes ... \otimes |\psi_N\rangle \tag{2.3}$$

The dimensionality of the Hilbert space of this system grows like 2^N with the number of qubits. The tricks we briefly introduced in the previous section rely on reducing the dimensionality of the problem. Basically your classical groundstate provides you with an anchor in this highly-dimensional Hilbert space and you only have to concern yourself with fluctuations near this anchor. In the case of long-range entanglement you have lost this anchor and you are faced with the entire Hilbert space dimensionality. This implies that classical computers require a computational time scaling like $exp(N)$. In condensed matter systems N can quickly be of order 10^{23}. A hopeless exercise demonstrated by the fact that state of the art computations have gone from computing these states for N=20 to N=25 particles over the course of the last 40 years.[11] Quantum computers offer hope in this regard that the complexity of such quantum mechanical problems might be reduced to polynomial times.

Version of July 4, 2022– Created July 4, 2022 - 20:01

We can make an argument that systems governed by quantum criticality as discussed in sect. 1.4 show long-range entanglement. After all, one of the defining features of critical states is the onset of scale-invariance. This goes hand-in-hand with the divergence of correlation length as a system approaches criticality. Large correlation lengths seem to suggest that particles throughout the system may be entangled. Luckily, as we have seen in the previous chapter, holography provides an alternative description to such strongly interacting quantum critical systems. The next section will connect quantum criticality and the strange metal and reveal promising leads that holography might offer a description.

2.3 Strange Metals

The nature of the strange metal phase has eluded a theoretical description for now. Strange metal's most characteristic property is a resistivity which scales linearly with temperature. However, linear resistivity can be found in nearly all metals due to electron-phonon coupling. What makes strange metals "strange" is that their resistivity does not saturate at the Mott-Ioffe-Regel (MIR) limit. This is the bound where the mean-free-path of a typical electron becomes of order of the crystal lattice spacing. Neither does it give in to $R \sim T^2$ at low temperatures before it goes superconducting. Figure (2.2) demonstrates the contrast with regular metals, where $T-$linear resistivity which can be ascribed to electron-phonon interactions, saturates at the MIR bound as electron-phonon interactions cannot reduce the mean-free-path to lengths shorter than the lattice constant. What makes strange metals *strange* is that linear resistivity proceeds well passed this bound. Clearly there must be another mechanism at work and the expected candidate is electron-electron interactions.

There are many indications that at least a portion of the strange metals are of the quantum critical strongly interacting kind. Figure 2.3 shows the phase diagram of the cuprate high-T_c superconductors. It is widely believed in the community that the phase diagram is governed by a quantum critical point at zero temperature and critical doping. In that case the strange metal phase should be the finite temperature state associated with criticality as discussed in 1.4.1. Indeed experiments have found response functions to demonstrate energy-temperature scaling [12]. Furthermore the momentum relaxation times responsible for the resistivity have been measured to be Planckian in a broad array of strange metals [13]. This suggests that quantum criticality is tied to the strange metal phase, but

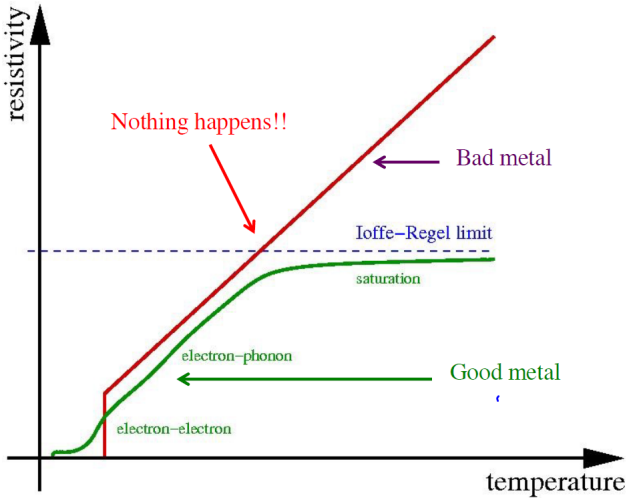

Figure 2.2: *Illustration of the deviations of strange metal resistivity behaviour from resistivity of conventional metals. Green displays a typical Fermi liquid metal. The red line is the resistivity curve of a strange metal. The resistivity of the strange metal does not saturate at the MIR bound. Source: [11]*

the evidence is not yet conclusive. Other mechanisms might saturate the Planckian bound without criticality necessarily being the culprit.

For the sake of argument, take for a moment, the assertion that the strange metal phase is governed by long-range entanglement to be true. In that case holography might offer physicists the best available description. In that case we can still describe the transport of the system, just not in terms of quasi-particles. We then should view transport as the flow of this holographic fluid in the presence of an ionic lattice. It has been argued in literature [15] that the effects of this hydrodynamic view should be observable as at short enough scales turbulent phenomena appear. These turbulent effects could not arise in quasi-particle description and provide the possibility of confirming or falsifying the claim that holography describes these systems. Confirmation would be a first step in further understanding the nature of the high-T_c superconducting state which arises in this strange metals at low temperature. As described in [16] it could be precisely the minimal viscosity associated with planckian dissipation which causes the superconducting state to persist to temperatures higher than expected from the regular BCS-paradigm.

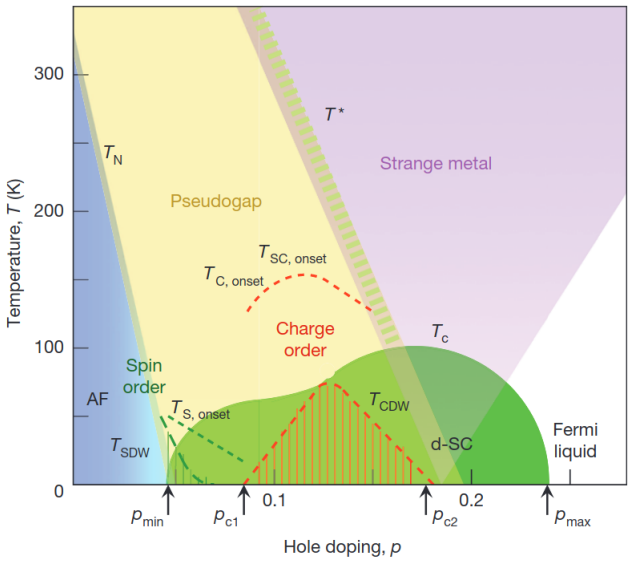

Figure 2.3: *Typical phase diagram of the cuprates. Displaying the high-T_c phase and the strange metal phase which are believed to be closely related to a zero temperature quantum critical point. Figure from:[14]*

2.4 Holographic strange metals

In the previous section some indications that holography might offer a description of strange metals has been mentioned. The work of this thesis is part of a group effort to create such a description. This is done starting from either the RN or GR model studied in this thesis and then introducing a charged lattice to the UV boundary conditions. The point is to create a model where the charged holographic fluid can dissipate momentum like it does in regular metals by interacting with an ionic lattice. Models which break translational symmetry have been studied before by introducing a lattice in the scalar field [17] or by introducing so-called holographic Q lattices [18]. Another approach which has been studied in this context are the holographic axion models which introduce extra scalar fields in the bulk action which couple to the gauge field and function as a momentum sink [19].

The main contrast in the approach taken by members of our group in [20–23] is that the lattice is introduced in the UV boundary of the gauge field, which causes the lattice to be charged. The lattice can then be seen as local fluctuations of the charge density in the UV theory attempting to replicate the effects of an ionic lattice in a metal. The results for the

"Gubser-Rocha"-metal [24] appear to be very promising as they replicate typical strange metal features such as T-linear resistivity over a large temperature and parameter range and even the development of a Mid-infrared peak which is common in the optical conductivity of strange metals.

Understanding the quasinormal modes of the homogeneous system is the starting point of a model where one explicitly breaks the symmetry. Many of the modes in the broken-translation system can be traced back to the quasinormal modes we study here. In the weak-symmetry breaking regime the effect of an umklapp potential on the dispersion relations we find in 3 can be calculated perturbatively. This allows the association of modes of the holographic strange metal with the global symmetries we define through hydrodynamics.

2.5 Conventional Transport theory

The aim is to describe the transport properties of the boundary CFT. Typically in condensed matter systems the transport of two quantities is of interest; Heat and charge. Of course these two quantities are not independent; An electron transports charge but it also carries heat. This leads us to write down the conductivity matrix 2.4. This should be read as the electric field $\overrightarrow{E}$ and the normalised temperature gradient $-\overrightarrow{\nabla}(T)/T$ sourcing both a heat ($\overrightarrow{Q}$) and a charge ($\overrightarrow{J}$) current.

$$\begin{pmatrix} \overrightarrow{J} \\ \overrightarrow{Q} \end{pmatrix} = \begin{pmatrix} \sigma & \alpha T \\ \alpha T & \bar{\kappa} T \end{pmatrix} \begin{pmatrix} \overrightarrow{E} \\ -\overrightarrow{\nabla}(T)/T \end{pmatrix} \tag{2.4}$$

σ is the electric conductivity, $\bar{\kappa}$ is the thermal conductivity and α is the thermo-electric conductivity representing the mixing of the two transport phenomena. In the absence of a temperature gradient one arrives at the familiar Ohm's law $\overrightarrow{J} = \sigma \overrightarrow{E}$. Note that the off-diagonal components of the conductivity matrix are equal in time-reversal-symmetric systems as the ones studied in this thesis. Note that elements of the conductivity matrix are simply the retarded Green's functions in case of an equilibrium. In section 4.3 we pull this matrix through the dictionary to obtain the CFT transport properties in terms of the bulk gravitational fields.

Version of July 4, 2022– Created July 4, 2022 - 20:01

Chapter 3

Hydrodynamics

Hydrodynamics was invented to describe the flow of everyday fluids and gases. Although it may not appear so at first instance, hydrodynamics is also perfectly suited to describe the long wavelength physics of black hole quasinormal modes. Quasinormal modes are long lived excitations in the perturbations of the gravitational theory. In truth the connection between gravity and hydrodynamics works to deeper levels than linear response. It was even discovered that through the holographic correspondence Einstein's theory of gravity encodes the full Navier-Stokes equations [25], a discovery named the "fluid-gravity" correspondence.

The requirements for hydrodynamics to be a suitable description of a system are as follows: The system thermalizes sufficiently rapidly and is near a thermal equilibrium. The second condition is that we are probing the response of the system at sufficiently long wavelengths. In practice this boils down to $k, \omega < T$ so that we do not probe length and time scales shorter than those associated with thermal equilibration. When ω and k become larger than the temperature we find that our system enters the conformal regime and our response function start to behave like power-laws, losing their scale. Finally, the described system must have globally conserved quantities. In our case the conserved quantities are energy, momentum and charge density of our holographic fluid.

3.1 Relativistic hydrodynamics

Now, a discussion of the relativistic hydrodynamics of our system will follow. For the sake of brevity the reader is referred to canonical material on the basics of hydrodynamics and response functions [26] and a thorough introduction to relativistic hydrodynamics [27] of which we will be closely following the parts relevant for our investigation. To be clear we are discussing hydrodynamics of normal relativistic fluids in the absence of a magnetic field.

We start with our conservation equations for energy, momentum and current which can simply be written down:

$$\partial_\mu T^{\mu\nu} = 0, \tag{3.1a}$$
$$\partial_\mu J^\mu = 0. \tag{3.1b}$$

The conservation of these quantities in the boundary is the result of respectively time and space translation symmetry in the bulk and the bulk $U(1)$ symmetry. We then choose our thermal equilibrium to be defined by our thermodynamic parameters u^μ, T, μ. We assume that these thermodynamic variables vary slowly in space and time, which allows us to preform a derivative expansion. So at zeroth order in derivatives the entire fluid is in equilibrium while including higher and higher order derivatives of the thermodynamic allows for a description of increasingly rapid local fluctuations from equilibrium. Keeping full generality we can decompose our conserved currents into the so-called constitutive relations:

$$T^{\mu\nu} = \mathcal{E} u^\mu u^\nu + \mathcal{P}\Delta^{\mu\nu} + (q^\mu u^\nu + q^\nu u^\mu) + t^{\mu\nu}, \tag{3.2a}$$
$$J^\mu = \mathcal{N} u^\mu + j^\mu. \tag{3.2b}$$

Here $\Delta^{\mu\nu} \equiv \eta^{\mu\nu} + u^\mu u^\nu$ is the projector with $\eta^{\mu\nu}$ the Minkowski metric. The new variables which we have introduced and suggestively named $\mathcal{E}, \mathcal{P}, \mathcal{N}, q^\mu, t^{\mu\nu}, j^\mu$ are at this point just some functions of the our thermodynamic variables to be determined. Our derivative expansion follows from expressing these in terms of derivatives of the thermodynamic variables to desired order. We will go to first order.

We work in the Landau frame [27] which sets $q^\mu = 0$ and chooses T and μ such that we associate $\mathcal{E} = \epsilon$ and $\mathcal{N} = n$. Which leaves $\mathcal{P}, t^{\mu\nu}$ and j^μ to be defined.

$$T^{\mu\nu} = \epsilon u^\mu u^\nu + p\Delta^{\mu\nu} - \eta\Delta^{\mu\alpha}\Delta^{\nu\beta}(\partial_\alpha u_\beta + \partial_\beta u_- \frac{2}{d}\eta_{\alpha\beta}\partial_\mu u^\mu) - \zeta\Delta^{\mu\nu}\partial_\lambda u^\lambda + \mathcal{O}(\partial^2) \tag{3.3a}$$

$$J^\mu = nu^\mu - \sigma_Q T\Delta^{\mu\nu}\partial_\nu(\frac{\mu}{T}) + \mathcal{O}(\partial^2) \tag{3.3b}$$

Here we have implicitly assumed the positivity of entropy production which implies the transport coefficients η, ζ and σ_Q are all positive. η is the shear viscosity, ζ is the bulk viscosity and σ_Q is a conductivity which is not associated with the bulk flow sometimes named the "incoherent"conductivity [28]. Eqs. 3.3 together with the conservation equations and thermodynamics of our theory now fully determine the hydrodynamics to first order. So we linearize around thermal equilibrium set by $v^i = 0, T = const, \mu = const$. Our thermodynamic variables become $\epsilon = \epsilon_0 + \delta\epsilon(t, \mathbf{x}), p_i = p_{0,i} + \pi_i(t, \mathbf{x})$ and $n = n_0 + \delta n(t, \mathbf{x})$. Putting together eqs. 3.1&3.3 we obtain the equations of motion for the hydrodynamic fluctuations. After transforming to Fourier space we obtain the following equations:

$$\partial_t\delta\epsilon + ik_x\pi_x = 0, \tag{3.4a}$$

$$\partial_t\pi^\parallel + ik_x\beta_1\delta\epsilon + ik_x\beta_2\delta n + \gamma_s\mathbf{k}^2\pi_x = 0, \tag{3.4b}$$

$$\partial_t\pi_i^\perp + \gamma_\eta\mathbf{k}^2\pi_i^\perp = 0, \tag{3.4c}$$

$$\partial_t\delta n + \frac{\bar{n}}{\bar{w}}ik_x\pi_x + \sigma_Q\alpha_1\mathbf{k}^2\delta\epsilon + \sigma_Q\alpha_2\mathbf{k}^2\delta n = 0. \tag{3.4d}$$

Where combinations of thermodynamic derivatives have been simplified into α_i and β_i specified in (eqs. 3.5).

$$\alpha_1 = \frac{\partial\mu}{\partial\epsilon} - (\frac{\mu}{T})(\frac{\partial T}{\partial\epsilon}) \tag{3.5a}$$

$$\alpha_2 = \frac{\partial\mu}{\partial n} - (\frac{\mu}{T})(\frac{\partial T}{\partial n}) \tag{3.5b}$$

$$\beta_1 = (\frac{\partial p}{\partial\epsilon})_n \tag{3.5c}$$

$$\beta_2 = (\frac{\partial p}{\partial n})_\epsilon \tag{3.5d}$$

One learns from Kovtun and Kadanoff & Martin [26, 27] that this determines the hydrodynamic retarded response functions in full generality. Eq. 3.4c decouples from the rest of the system. The equation has the form

of simple conservation equation and hence a diffusive response:

$$G^R_{\pi_y\pi_y}(\omega,\mathbf{k}) = \frac{\bar{w}\gamma_\eta \mathbf{k}^2}{i\omega - \gamma_\eta \mathbf{k}^2}, \tag{3.6}$$

Where the enthalpy density is introduced $\bar{w} = \bar{\epsilon} + \bar{p}$.

The decoupled system of equations is of the form:

$$\partial_t \phi_a(t,\mathbf{k}) + M_{ab}(\mathbf{k})\phi_b(t,\mathbf{k}) = 0, \tag{3.7}$$

where in this case $\phi_a = (\delta\epsilon, \pi_x, \delta n)$. We can identify the sources of these perturbations to be $\lambda_a = (\delta T/T, v_x, \delta\mu - \frac{\mu}{T}\delta T)$. The susceptibility matrix is then given by:

$$\chi_{ab} = \left(\frac{\partial\phi_a}{\partial\lambda_b}\right) = \begin{pmatrix} T(\frac{\partial\epsilon}{\partial T})_{\mu/T} & 0 & (\frac{\partial\epsilon}{\partial\mu})_T \\ 0 & \bar{w} & 0 \\ T(\frac{\partial n}{\partial T})_{\mu/T} & 0 & (\frac{\partial n}{\partial\mu})_T \end{pmatrix}. \tag{3.8}$$

Obtaining the responses of the system then amounts to solving the initial value problem of eq. 3.7. The general solution from [27] is (with indices suppressed):

$$G^R(z,\mathbf{k}) = -(1 + i\omega K^{-1})\chi, \tag{3.9}$$

Working this out we obtain the hydrodynamic functions of the form:

$$G^R_{ab}(\omega,\mathbf{k}) = \frac{F_{ab}(\omega,\mathbf{k})}{d(\omega,\mathbf{k})}, \tag{3.10a}$$

$$d(\omega,\mathbf{k}) = \omega^3 + i\omega^2\mathbf{k}^2(\gamma_s + \sigma_Q\alpha_2) - \omega\mathbf{k}^2 v_s^2 + i\sigma_Q\mathbf{k}^4(\alpha_1\beta_2 - \alpha_2\beta_1). \tag{3.10b}$$

Here F_{ab} is a poleless real function detailing the specifics of the different responses. Note that due to time-reversal invariance $F_{ab} = F_{ba}$. The pole structure of the response functions is described by $d(\omega,\mathbf{k})$. These poles which lie in the lower complex plane translate to long-lived excitation modes in the real part of the response; The quasinormal modes. We can see this by an example of a diffusion mode with pole dispersion $\omega = -iDk^2$. The purely diffusive part of the response is then given by

$$G(\omega,k) = \frac{F(\omega,k)}{\omega + iDk^2} \tag{3.11}$$

The real part of the response function then becomes:

$$\mathrm{Re}(G) = \frac{F\omega}{\omega^2 + (Dk^2)^2} \tag{3.12}$$

This is the well-known half-lorentzian lineshape centred at $\omega = 0$ associated with diffusion. The linewidth is set by Dk^2. Thus we see that the poles obtained from $d(\omega, \mathbf{k})$ fully determine the systems response up to F_{ab} which contains thermodynamic factors and factors of ω, k.

3.2 Hydrodynamic quasinormal modes

The poles are solutions to $d(\omega, \mathbf{k}) = 0$. Taking the $\mathbf{k} \to 0$ limit the poles of the response function are described by:

$$\omega = -iD_{\text{shear}}k^2 + \mathcal{O}(k^4), \tag{3.13a}$$

$$\omega = -iD_{\text{diff}}k^2 + \mathcal{O}(k^4), \tag{3.13b}$$

$$\omega = v_s k - i\Gamma k^2 + \mathcal{O}(k^4). \tag{3.13c}$$

We recognise two diffusive modes described by longitudinal diffusion coefficient D_{diff} which we will name the charge diffusion, transversal diffusion coefficient D_{shear} which we will name the shear diffusion and a sound mode described by speed of sound v_s and sound attenuation Γ. The expression in terms of thermodynamic quantities and transport coefficients is then:

$$D_{\text{diff}} = \left(\frac{sT}{\epsilon + p}\right)^2 \frac{(\alpha_2\beta_1 - \alpha_1\beta_2)}{v_s^2} \tag{3.14a}$$

$$D_{\text{shear}} = \frac{\eta}{\epsilon + p} \tag{3.14b}$$

$$v_s^2 = \frac{\partial p}{\partial \epsilon} \tag{3.14c}$$

$$\Gamma = \frac{\eta}{2(\epsilon + p)} \tag{3.14d}$$

$$\tag{3.14e}$$

In section 4.4 we use the thermodynamics of our holographic models to express these coefficients in terms of our model parameters μ and Q for RN and GR respectively.

Chapter 4

Methods and Calculations

4.1 Holographic set-up

Below we will detail how to set-up holographic computations and how to identify gauge invariant modes for the Gubser-Rocha black hole. The procedure is identical for Reissner-Nordström, but the equations are simplified, thus we will only provide the relevant results for RN. In [29, 30] Edalati et al. detail the method in the transverse and longitudinal sectors respectively for RN and we closely follow their approach.

EMD theories contain gravity, a scalar potential $V(\Phi)$, a $U(1)$ gauge field and a coupling by $Z(\Phi)$ of the two former. Following [31] we begin with a general EMD action:

$$S = \frac{1}{2\kappa^2}\int d^4x\sqrt{-g}[R - Z(\Phi)F^{\mu\nu}F_{\mu\nu} - \frac{3}{2}(\partial_\mu\Phi)^2 + V(\Phi)]. \tag{4.1}$$

From this action one can obtain by principle of least action the following equations of motion (EOMs). Where we have substituted $\Phi = \frac{\phi}{\sqrt{3}}$ to obtain EOMs in a desirable form:

$$0 = R_{\mu\nu} - \frac{1}{2}Z(\phi)(F_{\mu\sigma}F^{\sigma}_{\nu} - \frac{1}{4}F^2 g_{\mu\nu}) - \frac{1}{2}\partial_\mu\phi\partial_\nu\phi + g_{\mu\nu}V(\phi) \tag{4.2}$$

$$0 = \nabla_\mu(Z(\phi)F^{\mu\nu}) \tag{4.3}$$

$$0 = \Box^2\phi - \frac{\sqrt{\phi}}{12}Z(\phi) + 2V'(\phi) \tag{4.4}$$

When one chooses $V(\phi) = cosh(\frac{\phi}{\sqrt{3}})$ and $Z(\phi) = e^{\frac{\phi}{\sqrt{3}}}$ Gubser and Rocha presented an analytic solution in [9] given by:

$$\begin{aligned} A_t(z) &= \frac{\sqrt{3Q(Q+1)}(1-z)}{Qz+1} \\ \phi(z) &= \frac{\sqrt{3}}{2}\log(Qz+1) \\ ds^2 &= \frac{1}{z^2}(-dt^2 f(z) + g(z)(dx^2+dy^2) + \frac{dz^2}{f(z)}) \end{aligned} \tag{4.5}$$

Where we have set L=1 and $\kappa = \frac{1}{\sqrt{2}}$.

$$\begin{aligned} f(z) = (1-z)\frac{p(z)}{g(z)}, g(z) &= (1+Qz)^{3/2} \\ p(z) = 1 + (1+3Q)z + (1+3Q(1+Q))z^2 & \end{aligned} \tag{4.6}$$

Here we have chosen coordinates such that the horizon is at z=1 and the boundary is at z=0. The chemical potential μ is identified as $\mu = A_t(z = 0)$. The Hawking temperature is then set by the inverse periodicity of the metric at the horizon, as we derived in eq. 1.5, which yields for the Gubser-Rocha black hole:

$$\begin{aligned} \frac{T}{\mu} &= \frac{\sqrt{3}}{4\pi\sqrt{Q}} \\ \mu &= \sqrt{3Q(1+Q)} \end{aligned} \tag{4.7}$$

The details of the Reissner-Nordström black hole are given in A.

4.2 Gauge-invariant modes

To investigate the response of our model we add perturbations γ' to all our background fields $\gamma^{(0)}$ such that the total fields become:

$$g_{\mu\nu} = g^{(0)}_{\mu\nu} + \epsilon h_{\mu\nu}\exp(ikx - i\omega t) \tag{4.8}$$

$$A_\mu = A^{(0)}_\mu + \epsilon a_\mu \exp(ikx - i\omega t) \tag{4.9}$$

$$\phi = \phi^{(0)} + \epsilon\psi\exp(ikx - i\omega t) \tag{4.10}$$

Version of July 4, 2022– Created July 4, 2022 - 20:01

. Our perturbation fields are $h_{\mu\nu}, a_\mu, \psi$ for respectively the metric, gauge and scalar fields perturbations. We work in the radial gauge which sets $h_{\mu z} = a_z = 0$. The radial gauge does not completely fix the gauge freedom of our system. Drawing inspiration from [29] we set out to reduce the number of fields in our equations by choosing combinations which are invariant under gauge (eq 4.11) and diffeomorphism transformation (eq 4.12).

$$A_\mu \to \tilde{A}_\mu = A_\mu + \nabla_\mu \chi \tag{4.11}$$
$$\psi \to \tilde{\psi} = \psi - \chi^\lambda \nabla_\lambda \beta$$
$$h_{\mu\nu} \to \tilde{h}_{\mu\nu} = h_{\mu\nu} - (\xi^\lambda \nabla_\lambda \tilde{g}_{\mu\nu} + \tilde{g}_{\lambda\nu}\nabla_\mu \xi^\lambda + \tilde{g}_{\mu\lambda}\nabla_\nu \xi^\lambda) \tag{4.12}$$
$$a_\mu \to \tilde{a}_\mu = a_\mu - (\xi^\nu \nabla_\nu \tilde{A}_\mu + \tilde{A}_\nu \nabla_\mu \xi^\nu)$$

The condition for invariance under transformations 4.11 & 4.12 for any χ, β, ξ^μ provides 10 equations to satisfy which can be solved up to 5 remaining degrees of freedom. These 5 independent solutions are gauge invariant combinations of the original perturbations. In the transverse (vector) sector we obtain modes:

$$E_y = \omega a_y \tag{4.13}$$
$$Z_y = k h_{ty} + \omega h_{xy} \tag{4.14}$$

And in the longitudinal (scalar) sector:

$$E_x = k a_t + \omega a_x + \frac{k z h_{yy} A_t'(z)}{2g(z) - z g'(z)}$$
$$Z_x = \frac{k^2 h_{yy}(z f'(z) - 2f(z))}{z g'(z) - 2g(z)} + k^2 h_{tt} + 2k\omega h_{tx} + \omega^2 (h_{xx} - h_{yy}) \tag{4.15}$$
$$Z_\eta = \frac{h_{yy}\phi'(z)}{2g(z) - z g'(z)} + \psi(z) \tag{4.16}$$

Rewriting the equations of motion in terms of the gauge-invariant modes the equations decouple into the two sectors; Transverse and longitudinal to the perturbation wavevector. Similar equations of motion in terms of the gauge-invariant modes may be found for the Reissner-Nordström

black hole in work by Edalati [29, 30]. The problem at hand has now been reduced to two independent sets of coupled differential equations of 5 fields.

4.3 Holographic transport

The GKPW dictionary tells us that vevs and sources of operators in the boundary are set by the leading and sub-leading term in the boundary expansion of the dual bulk fields. [32] provides a good introduction for calculating the response of fields in the case of RN. We follow the methodology closely:

For some field ϕ the boundary expansion (near $z = 0$) is:

$$\phi(z) = \phi_{(0)} + z^{\Delta}\phi_{(1)} + ... \quad \text{as} \quad z \to 0. \tag{4.17}$$

This is obtained after rescaling the field such that the leading order is zeroth order in Z. The order Δ of the subleading term is dependant on the type of field. For our set-up metric fields have $\Delta = 3$ and both gauge fields and scalar fields have $\Delta = 1$. Due to this rescaling we can simply identify the source term $\phi_{(0)}$ with our UV boundary condition on ϕ. After solving the equations of motion numerically the VEV of a field, $\phi_{(1)}$, can be accessed by evaluating the Δ-th derivative of ϕ near the boundary. The retarded response of the dual operator in the CFT is then given by:

$$G^{R}_{\phi\phi} = \frac{\text{VEV}}{\text{src}} = \frac{\phi_{(1)}}{\phi_{(0)}} \tag{4.18}$$

At this point we note that the boundary values of the leading and subleading order of fields are under some constraints imposed by the UV of the system. This yields relations between VEV's and sources called Ward-identities which we discuss in Appendix B.

4.3.1 Holographic Thermo-electric conductivities

To compute the thermo-electric response of our boundary CFT we would like to use the dictionary to translate eq. 2.4 to be in terms of our bulk fields. As [32] details the "holographic" version of eq. 2.4 in terms of our field perturbations $h_{\mu\nu}, b_{\mu}$ is:

$$\begin{pmatrix} \langle J \rangle \\ \langle Q \rangle \end{pmatrix} = \begin{pmatrix} \sigma & \alpha T \\ \alpha T & \bar{\kappa} T \end{pmatrix} \begin{pmatrix} i\omega(\delta b_{x(0)} + \mu \delta g_{tx(0)}) \\ i\omega \delta g_{tx(0)}, \end{pmatrix} \tag{4.19}$$

Version of July 4, 2022– Created July 4, 2022 - 20:01

The right side of the equation details the sources of the temperature gradient $Q_x = \delta g_{tx(0)}$ and current $J_x = \delta b_{x(0)} + \mu \delta g_{tx(0)}$. As one would expect from the dictionary the gauge field is associated with the flow of charge while the tensor perturbation is associated with the flow of energy and temperature. The fact that $\delta g_{tx(0)}$ pops up in the source of the current as well is natural. In a normal metal a temperature gradient will also cause charge to flow. The thermo-electric conductivities can then be expressed in terms of the bulk field response:

$$\sigma(\omega, k) = \frac{-iG^R_{J_x J_x}(\omega, k)}{\omega}, \tag{4.20a}$$

$$\alpha(\omega, k)T = \frac{-iG^R_{Q_x J_x}(\omega, k)}{\omega}, \tag{4.20b}$$

$$\bar{\kappa}(\omega, k)T = \frac{-iG^R_{Q_x Q_x}(\omega, k)}{\omega}. \tag{4.20c}$$

From [28] we learn that we can extract the hydrodynamic transport coefficients from our holographic calculations independently of k:

$$\sigma_Q = \lim_{\omega \to 0} \frac{\mathrm{Im}\, G_{J_x J_x}(\omega))}{\omega} \tag{4.20d}$$

$$\eta = \lim_{\omega \to 0} \frac{\mathrm{Im}\, G_{T_{xy} T_{xy}}(\omega))}{\omega} = \lim_{\omega \to 0} \frac{\mathrm{Im}(G_{Z_y Z_y}(\omega, k = 0))}{\omega} \tag{4.20e}$$

4.4 Hydrodynamic predictions for RN & GR

In this section we apply what we have learnt from chapter 3 to the specifics of our RN and GR model. We need to identify the transport coefficients σ_Q, η and compute the relevant thermodynamic derivatives to obtain the diffusion constants D_l, D_t and the sound mode properties v_s, Γ.

As discussed in section 1.4.1 holographic theories at criticality have generally been found to have minimal shear viscosity equal to [33]:

$$\eta = \frac{s}{4\pi}. \tag{4.21}$$

Furthermore the thermodynamic expression for the incoherent conductivity is since we are working in 2 spatial dimensions [28]:

$$\sigma_Q = \left(\frac{s}{4\pi}\right)^{\frac{d-2}{d}} \left(\frac{sT}{\epsilon + p}\right)^2 = \left(\frac{sT}{\epsilon + p}\right)^2 \tag{4.22}$$

The first law of thermodynamics of our system is given by:

$$\epsilon + p = \mu\rho + sT. \tag{4.23}$$

Which we can use to compute thermodynamic derivatives. This leaves the entropy and the energy and momentum density as unknown quantities. The entropy is set by the Bekenstein-Hawking entropy of the black hole. By Bekenstein-Hawking the entropy is proportional to the black hole area which we obtain by integrating the area differential at the horizon over the polar coordinates. Thus we obtain in terms of the spatial part of the metric g_{ij}:

$$s = 4\pi\sqrt{|g_{ij}|}, \tag{4.24}$$

Thus we obtain for GR and RN respectively:

$$s_{GR} = 4\pi(1+Q)^{1/3} \tag{4.25}$$

$$s_{RN} = 4\pi \tag{4.26}$$

The energy and momentum density of our CFT can be obtained from the energy momentum tensor in the boundary. This requires the derivation from the boundary action, which we do in the following subsection. The energy density is then set by value of T^{tt} and the momentum density by T^{xx}. Energy and momentum density are related simply by $\epsilon = 2p$ in conformal invariant systems.

For GR we obtain:

$$\epsilon_{GR} = 2(1+Q)^3, \tag{4.27}$$

For RN we obtain:

$$\epsilon_{RN} = \frac{4+\mu^2}{2} \tag{4.28}$$

Taking all these identities together with the hydrodynamic prediction of the transport coefficients eqs. 3.14. We obtain our hydrodynamic predictions for the quasinormal modes in terms of our model parameters:

$$D_{\text{diff,GR}} = \frac{1}{(1+Q)^{3/2}} \tag{4.29a}$$

$$D_{\text{shear,GR}} = \frac{1}{3(1+Q)^{3/2}} \tag{4.29b}$$

$$\Gamma_{\text{GR}} = \frac{1}{6(1+Q)^{3/2}} \tag{4.29c}$$

For RN we obtain

$$D_{\text{diff,RN}} = \frac{1}{3} + \frac{8}{3(4+\mu^2)} \tag{4.30a}$$

$$D_{\text{shear,RN}} = \frac{4}{3(4+\mu^2)} \tag{4.30b}$$

$$\Gamma_{\text{RN}} = \frac{2}{3(4+\mu^2)} \tag{4.30c}$$

And the speed of sound for both our RN and GR set-up is equal to:

$$v_s = \frac{1}{\sqrt{2}} \tag{4.31}$$

4.4.1 Energy momentum Tensor of the boundary CFT

To describe the hydrodynamics of our boundary theory we need to obtain a stress tensor for it. Normally the energy-momentum tensor of a theory is obtained by varying the action with respect to the metric. We can simply follow that procedure if we identify a boundary action. The action of our boundary CFT is set by the boundary terms originating from integrating the bulk action by parts and counter-terms which regularize the on-shell action. Specfically the Gibbons-Hawking-York boundary term regularizes the Einstein-Hilbert action on shell. Following [34] we define our action including counterterms:

$$S = \int dx^4 \mathcal{L}_{GR} + \oint dx^3 \mathcal{L}_{\text{GHY}} \tag{4.32}$$

On the UV boundary we only have to worry about the Einstein-Hilbert part of our Gubser-Rocha Lagrangian. We obtain the energy momentum tensor by varying the action with respect to the metric induced on the boundary $\gamma_{\mu\nu} = g_{\mu\nu} - n_\mu n_\nu$. Here n_μ is the normal one form which defines the hypersurface of our boundary. We obtain:

$$\delta S = \frac{-1}{2\kappa^2} \oint dx^3 \sqrt{-\gamma} \delta\gamma^{\mu\nu} \left(R_{\mu\nu} + 2\gamma_{\mu\nu} + K_{\mu\nu} - \gamma_{\mu\nu} K \right), \tag{4.33}$$

Where K is the extrinsic curvature of the submanifold and $R_{\mu\nu}$ here is the Ricci tensor on the submanifold. The 4-dimensional extrinsic curvature $K'_\mu\nu$ is defined as:

$$K'_{\mu\nu} = -\frac{1}{2}(\nabla_\mu n_\nu + \nabla_\nu n_\mu) \tag{4.34}$$

Version of July 4, 2022– Created July 4, 2022 - 20:01

The 3-dimensional extrinsic curvature on our hypsersurface is then:

$$K_{\mu\nu} = \gamma^{\alpha}_{\mu}\gamma^{\beta}_{\nu}K'_{\alpha\beta} \tag{4.35}$$

Putting these expression together we obtain the boundary energy-momentum tensor:

$$T_{ij} = \frac{2}{\sqrt{-\gamma}}\frac{\delta S}{\gamma^{ij}} = \frac{-1}{\kappa^2}(K_{ij} - K\gamma_{ij} + R_{ij} + 2\gamma_{ij}) \tag{4.36}$$

Taking $\kappa = \frac{1}{\sqrt{2}}$ and inserting the GR and RN metric respectively yields diagonal tensors with the energy density given by eqs. 4.27, 4.28. Both energy-momentum tensors are traceless as they should be in conformal systems and thus obey $\epsilon - 2p = 0$.

4.5 Numerics

Two numerical methods have been employed to obtain results. One approach uses the ”holographic lattice code” written by F. Balm [24]. This method was used when computing high temperature thermo-electric conductivities of the system. The second approach used was the iterative Generalised Minimal Residual Method of the Mathematica Krylov solver [35]. The advantage of Mathematica it allows the user to specify number precision. This is particularly relevant for low temperature calculations in Gubser-Rocha as model parameter Q starts to take large values and machine precision is no longer adequate. The trade-off is that the mathematica algortihm solver is slower.

Both techniques iteratively solve differential equations on a grid using finite-difference techniques. [36] gives an introduction to the techniques used by the holographic lattice code for the interested reader. The grid on which the PDE's were solved was of the Chebyshev kind. The Chebyshev lattice spaces the gridpoints on a domain $z : (0, 1)$ with a density described by $\cos(z\pi)$. There are two reasons why this is useful; First of all the bulk fields vary most rapidly near the horizon and the boundary, thus increased gridpoints in these regions increases accuracy in the found solution. Secondly, the high density of gridpoints near the boundary increases accuracy in the first three derivatives of our fields which we read out to obtain our VEV and source.

Version of July 4, 2022– Created July 4, 2022 - 20:01

Chapter 5

Results

5.1 Thermo-electric response

The plots of the thermo-electric conductivities which we obtain by the method explained in section 4.3 can be found in Appendix C. The results have been put in the appendix since the responses submit entirely to the responses set by the hydrodynamic transport coefficients and modes. One response is interesting enough to highlight here, the thermal conductivity in absence of a current κ.

$$\kappa = \bar{\kappa} - \frac{\alpha^2 T}{\sigma} \tag{5.1}$$

We observe that both in Gubser-Rocha and Reissner-Nordström this conductivity is 0. This implies that the system cannot dissipate energy without a current starting to flow.

5.2 Hydrodynamic Transport coefficients

As discussed in section 4.3 we can obtain our hydrodyanamic transport coefficients σ_Q and η from bulk calculations of the retarded responses. In terms of the response-functions of our gauge-invariant modes we have:

$$\sigma_Q = \mathrm{Re}(\sigma(\omega \to 0, k = 0)), \tag{5.2}$$

$$\eta = \lim_{\omega \to 0} \frac{\mathrm{Im}(G_{Z_x Z_x}(\omega, k = 0))}{\omega} = \lim_{\omega \to 0} \frac{\mathrm{Im}(G_{Z_y Z_y}(\omega, k = 0))}{\omega}. \tag{5.3}$$

Note that at $k = 0$ our system is isotropic in the spatial directions and it thus does not matter whether we take the response of Z_y or Z_x. Figure

5.1 shows that the incoherent conductivity matches perfectly the thermodynamic predictions from section 4.4. Likewise figure 5.2 shows that the shear viscosity is in agreement with thermodynamic predictions as well.

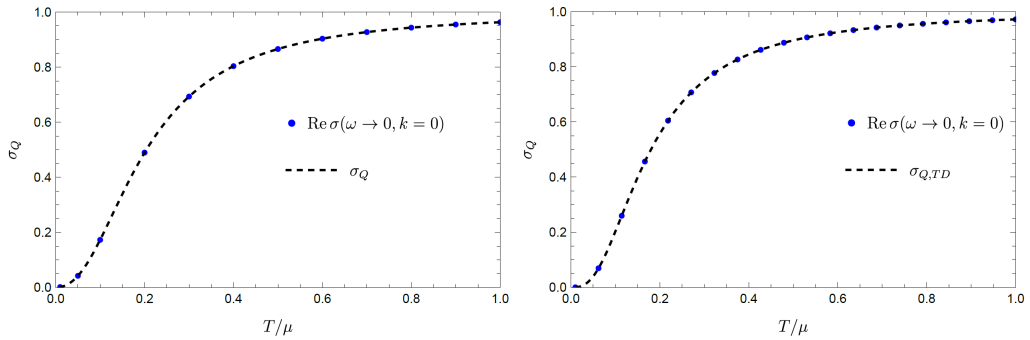

Figure 5.1: *Figures displaying incoherent conductivity σ_Q as obtained from thermodynamic prediction dashed and holographic calculation dots.*

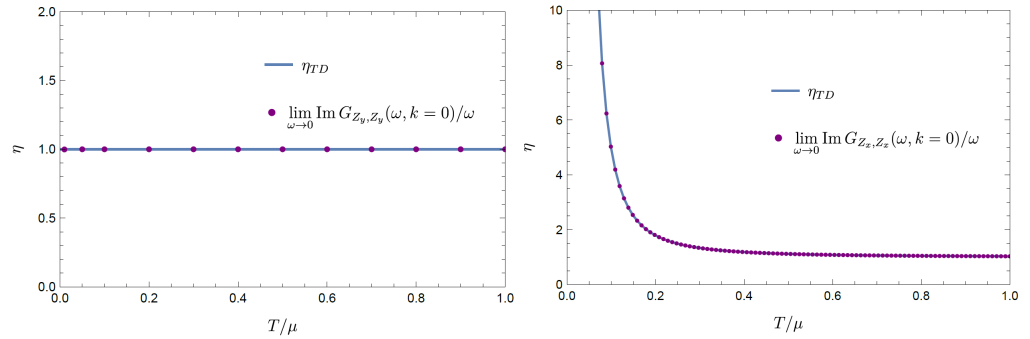

Figure 5.2: *Figures displaying shear viscosity η as obtained from thermodynamic prediction full and holographic calculation dots.*

5.3 Hydrodynamic modes

Now the identification of constants describing the diffusive and sound modes of our system. In the hydrodynamic limit these fully describe the response of the system as the responses the different modes can be expressed in terms of each other using continuity equations. An example is given by the conservation of charge $\partial_\mu J^\mu = 0$. This implies that we can relate the charge density response to the current response by:

$$\omega^2 G^R_{J^t J^t} = k^2 G^R_{J^x J^x} \tag{5.4}$$

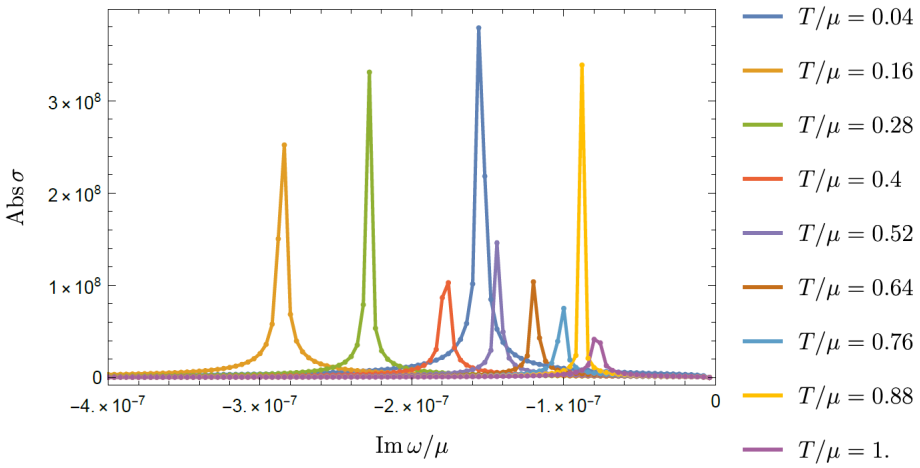

Figure 5.3: *Figure demonstrating how the diffusive poles are identified at different temperatures in the transverse sector. Lines are drawn between between data points for clarity.*

Since we know from eqs. 3.13 that the diffusive poles lie on the imaginary ω axis we can compute response functions which should contain these modes along the imaginary axis to observe the poles. Fig. 5.3 shows what this looks like for a typical set-up. These responses have no direct physical meaning as imaginary frequency cannot be probed in the physical world, but it allows us to easily identify the position of the poles in the imaginary plane.

We probe the diffusive mode by studying the conductivities in both the transverse and longitudinal sector along the imaginary ω axis. The conductivities in terms of the gauge-invariant perturbations are given by:

$$\sigma_y = \frac{\omega^2}{\omega^2 - k^2} \frac{-iG_{E_y E_y}(\omega, k)}{\omega}, \tag{5.5}$$

$$\sigma_x = \frac{\omega^2}{k^2 - \omega^2} \frac{-iG_{E_x E_x}(\omega, k)}{\omega}. \tag{5.6}$$

We probe the shear diffusion through the transverse conductivity σ_y and we probe the charge diffusion and sound mode through the longitudinal conductivity σ_x. The pre-factors in eqs. 5.5 and 5.6 come from rewriting the conductivity in terms of the gauge-invariant perturbations.

Our computations are all done for parameters in units of μ. Recall that the position of the diffusive pole is set by $\omega = -iDk^2 + \mathcal{O}(k^4)$ which

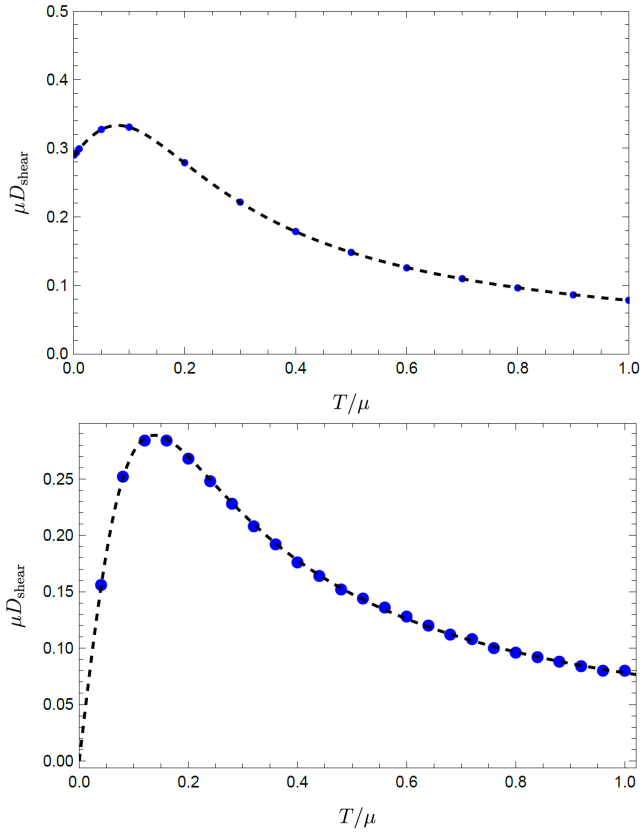

Figure 5.4: *Figures displaying shear diffusion as obtained from thermodynamic prediction dashed and holographic calculation dots.*

means if we take the position ω/μ along the imaginary axis of a pole and divide out the value of $(k/\mu)^2$ we obtain an estimate of the diffusion constant μD which we plot in for the transverse case in fig. 5.4 and the longitudinal case in fig. 5.5.

We observe a deviation from the thermodynamic predictions in Gubser-Rocha at low temperatures in the charge diffusion mode. In the next chapter we will discuss the expected reason for the deviation.

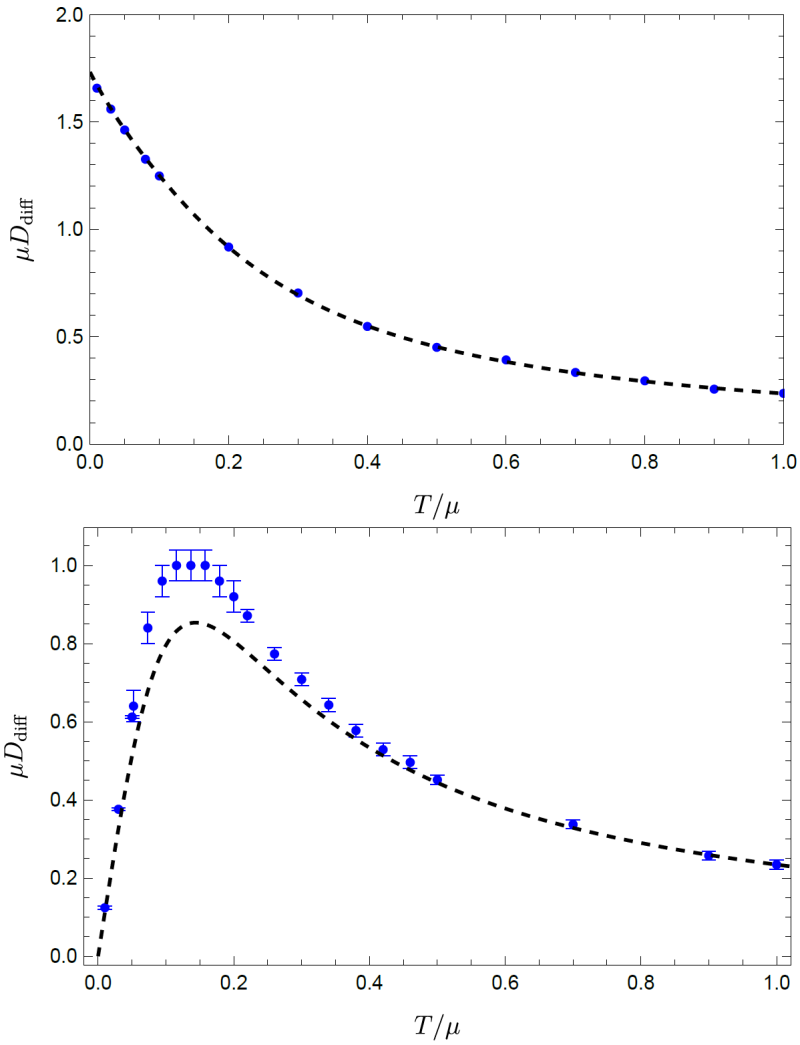

Figure 5.5: *Figures displaying (longitudinal) charge diffusion as obtained from thermodynamic prediction dashed and holographic calculation dots. Errorbars are obtained by taking the error to be the size of the ω/μ-spacing in identifying the poles (fig. 5.3).*

Finally to obtain the speed of sound v_s and the sound attenuation Γ of our system we analyse the real response of the conductivity in the longitudinal direction. The reason for not repeating the same procedure as for the diffusive modes along a line into the imaginary axis at the speed of sound is that we found the speed of sound to be varying in Gubser-Rocha.

The alternative approach taken was to make a fit of the sound peak. The central position of the peak should then correspond to $\omega = v_s k = \frac{v_s}{\sqrt{2}}$. The width of the peak should then be set by the sound attenuation. The fitting function used is that of a lorentzian lineshape:

$$\mathrm{Re}(\sigma) = \frac{\sigma_0(\omega - v_s k)}{\Gamma^2 k^4 + (\omega - v_s k)^2}, \tag{5.7}$$

This is obtained from considering a response dominated by the sound pole such that $\sigma = \frac{\sigma_0}{\omega - v_s k - i\Gamma k^2}$. σ_0 is a dummy parameter and not of interest in this case as we wish to derive the sound attenuation and speed of sound. Figures 5.7 and 5.8 then show the results of the speed of sound and the sound attenuation respectively. It is interesting to note that we observe low temperature deviations from the thermodynamic predicitions in Gubser-Rocha once again.

Version of July 4, 2022– Created July 4, 2022 - 20:01

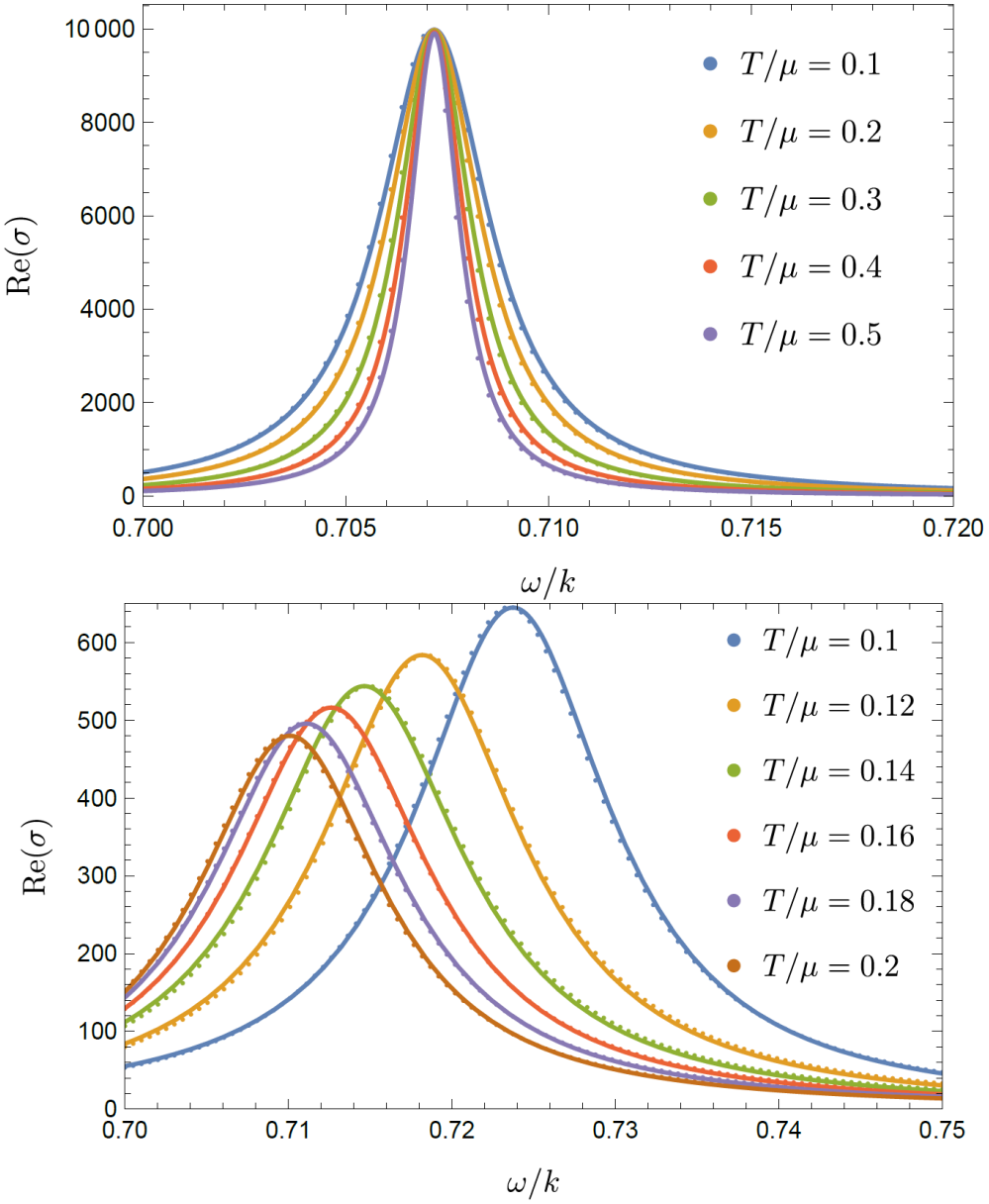

Figure 5.6: *Figures displaying the fits made to the real axis sound peaks to obtain the position and width of the peak. Data taken at k/μ=0.05. top: RN bottom: GR.*

Version of July 4, 2022– Created July 4, 2022 - 20:01

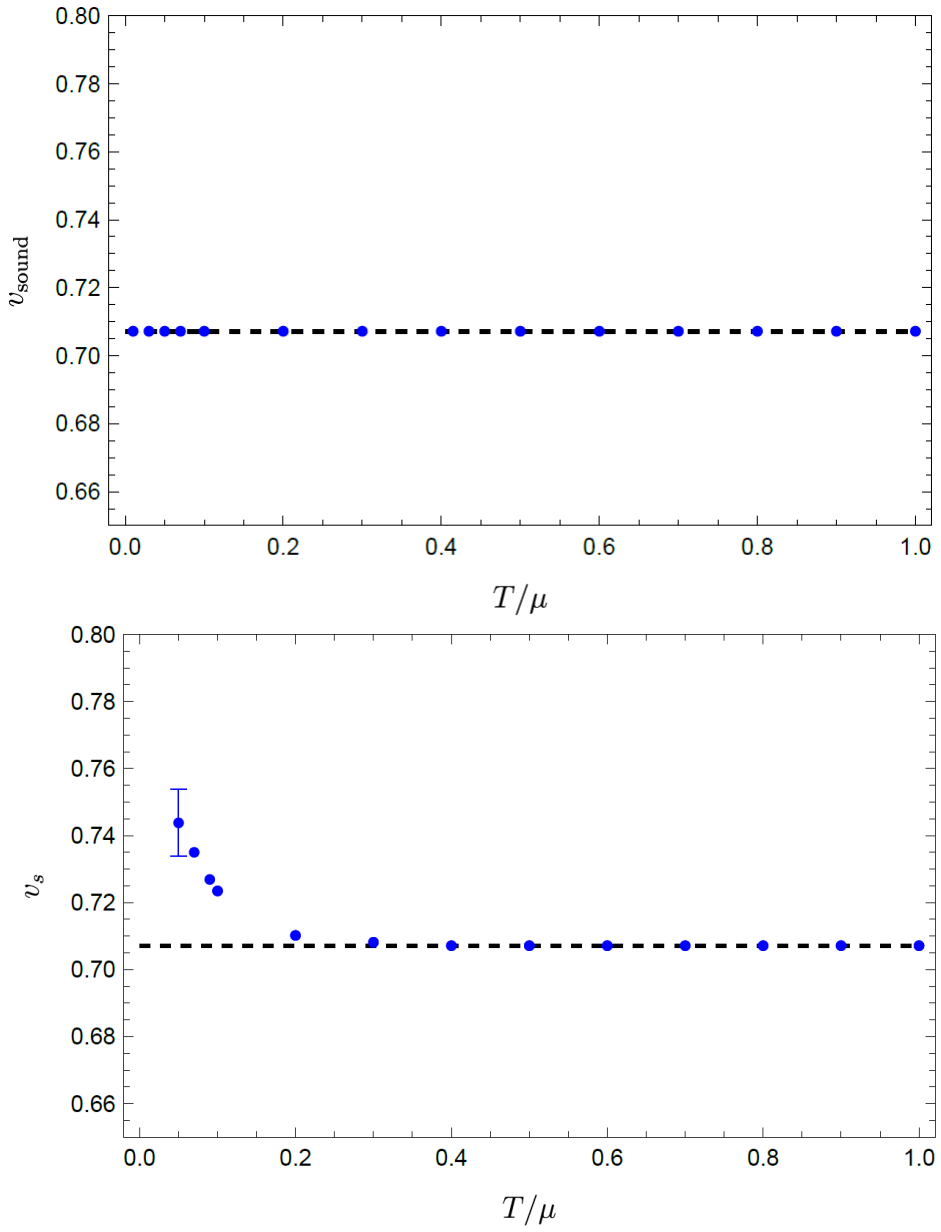

Figure 5.7: *Figures displaying the speed of sound as obtained from thermodynamic prediction dashed and holographic calculation dots.*

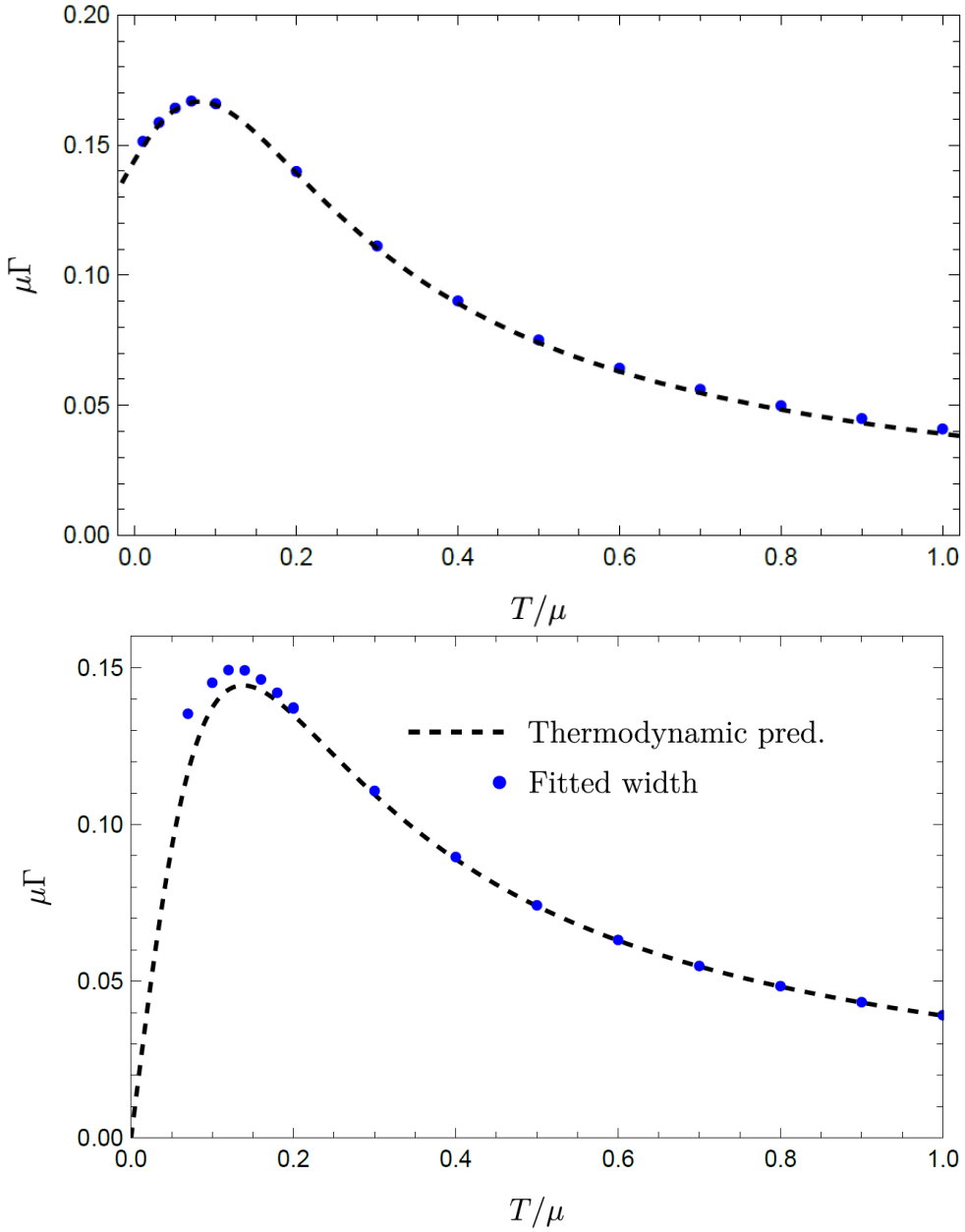

Figure 5.8: *Figures displaying the sound attenuation as obtained from thermodynamic prediction dashed and holographic calculation dots.*

Chapter 6

Discussion

We have studied the quasinormal modes of the Gubser-Rocha black hole and compared the results with the quasinormal modes of the Reissner-Nordström black hole. Hydrodynamics offer predictions for the long wavelength behaviour of these quasinormal modes and the agreement is perfect in the case of RN. We observe that the agreement is good for a large range of temperatures in GR as well. However, at temperatures below $T/\mu = 0.2$ we start to see deviations from the prediction in the longitudinal sector; The charge diffusion mode, speed of sound and sound attenuation all show deviations.

We believe we have found the cause of the discrepancy, although this could not be fixed in time to correct the results in this thesis. The attentive reader may have observed that we do not take into account a contribution of the scalar field in our thermodynamic considerations. This is suspected to be the cause of the trouble. The Gubser-Rocha solution sets the values of T and μ at a given parameter Q as specified in equation 4.7. As explained by [34] one can generalise the system's thermodynamics to include a set of conjugate variables for the scalar field. Unfortunately the Gubser-Rocha solution does not allow one to freely vary the scalar parameter; One can view the thermodynamic parameters as a 3-dimensional phase space with coordinates (T, μ, ϕ^*) in which the Gubser-Rocha solution allows one to access a 1-d line of solutions by varying Q which fixes the value of T/μ. Implicitly this should fix ϕ^* as well but it is presently unclear how to obtain ϕ^*. For this reason the Gubser-Rocha black hole solution seems unsuitable for this approach where one generalises the thermodynamics to include the scalar contribution.

Version of July 4, 2022– Created July 4, 2022 - 20:01

The alternative is to choose a quantisation in which the scalar field does not contribute to the thermodynamics. Kim et al. [34] nicely explain how to make a choice of quantisation in holographic EMD-theories. The quantisation is set by an appropriate choice of boundary counter-terms in the action containing the scalar field. This in turn, imposes non-trivial boundary conditions on the scalar field ϕ. Whereas we have taken boundary condition $\phi = 0$ when not sourcing the scalar field, it turns out the actual boundary condition should have the form $\phi' + c\phi^2 = 0$ for some to be determined parameter c. The implication for results we have shown for Gubser-Rocha in this thesis is that they have inadvertently included sourcing of the scalar field.

This explains why the deviations we have found do not show up when looking at the shear-diffusion mode. As we have seen in section 4.2 the transverse sector E_y and Z_y completely decouple from the scalar field. For this reason the accidental sourcing of the scalar field does not couple to the transverse fields and we get away with ignoring ϕ in the thermodynamic consideration.

Chapter 7

Conclusion & Outlook

Naturally, the first order of business when proceeding should be to confirm that the considerations discussed in the previous chapter indeed fix the discrepancy we observe. Beside that we have identified the gauge-invariant modes of the Gubser-Rocha black hole, which greatly simplify the computation of responses. The Gubser-Rocha black hole is not particularly well-suited for low temperature numerical computations. Since $Q \sim \frac{1}{(T/\mu)^2}$, Q becomes very large at low temperatures and numerical accuracy suffers as a result. By doing the bulk calculations in terms of the gauge-invariant modes the temperature can be lowered significantly further before this becomes an issue.

The understanding of the quasinormal modes in terms of the hydrodynamic description is of great interest to future research. Particularly in the study of the Gubser-Rocha strange metal. Preliminary results by [24] indicate that in the presence of a weak potential lattice the quasinormal modes described in this thesis may be "Umklapped" by the potential lattice. This allows the response modes of the Gubser-Rocha strange metal to be traced back to the shear diffusion, charge diffusion and sound mode analysed here. This is promising as the Gubser-Rocha strange metal appears to display many features which characterise the strange metal from a Sommerfeld entropy to a mid-infrared peak appearing in the optical conductivity. [22–24] The holographic strange metal models provide a template with which to further study the connection between holography and the strange metal. One apparent follow up step would be to introduce a magnetic field in the models as was done in Reissner-Nordström in [21]. The introduction of a magnetic field increases richness of the responses. These responses can also be compared be compared to a range of exper-

imental findings of transport phenomenon in strange metals in the presence of magnetic fields.

Holographic models with ionic lattices are now actively being studied for the Reissner-Nordström black hole and the Gubser-Rocha black hole solutions. A reason for this is that both models have the property that they are locally quantum critical $z \to \infty$, which relates them to the strange metal. It would be very interesting to generalise these investigations to holographic models at arbitrary quantum critical exponents z, θ. How these critical exponents control the systems response is of great interest to obtain a broader understanding of the holographic duality. This research and that of coworkers [20–24] can serve as a template for such further investigations.

Appendix A

Reissner-Nordström solution and Gauge-invariant modes

We find the same Reissner-Nordström solution and gauge invariant modes as [29, 30]. Be aware that Edalati et al. use an inverted radial coordinate with repect to ours. The Reissner-Nordström solution is set by (after having taken L=1 and $\kappa = \frac{1}{\sqrt{2}}$):

$$ds^2 = \frac{1}{z^2}\left(-f(z)dt^2 + dx^2 + dy^2\frac{1}{f(z)}\right) \tag{A.1}$$

$$A_t = \mu(1-z) \tag{A.2}$$

$$f(z) = 1 - (1+\mu^2/4)z^3 + \frac{\mu^2 z^4}{4} \tag{A.3}$$

By using eq. 1.5 we obtain RN temperature:

$$T = \frac{\mu^2 - 12}{16\pi} \tag{A.4}$$

The gauge-invariant modes of Reissner-Nordström are given by (in the up-down representation):

$$E_y = \omega b_y \tag{A.5a}$$

$$Z_y = \omega h^x_y + k h^y_t \tag{A.5b}$$

$$E_x = k b_t + \omega b_x - \frac{kz\mu}{2} h^y_y \tag{A.5c}$$

$$Z_x = 2k\omega h^x_t + \omega^2(h^x_x - h^y_y) + k^2 f(z)(h^y_y - h^t_t) - \frac{zk^2}{2} f'(z) h^y_y \tag{A.5d}$$

Do to the absence of the scalar field RN has one less degree of freedom than GR.

Appendix B

Gubser-Rocha Ward identities

By solving the UV boundary series expansion order by order we obtain the following Ward identities for our perturbations $h_{\mu\nu}$, b_μ and η:

$$\begin{aligned}48\left(\frac{k^2-\omega^2}{\omega}\right)h_{tx(3)} &= 16\mu Q(k*b_{t(0)}+\omega*b_{x(0)})\\ &+6(-4+3Q(-4+k^2)-12Q^2-4Q^3)(kh_{tt(0)})-2\omega h_{tt(0)}+\\ &6k(4+12Q^2+4Q^3+12Q-3Q\omega^2)(h_{xx(0)}+h_{yy(0)})+18kQ^3h_{yy(0)}\\ &+48kh_{yy(3)}-5\sqrt{3}kQ^2\eta_{(0)}\end{aligned}\tag{B.1}$$

$$\begin{aligned}\left(k^2-\omega^2\right)(48h_{tt(3)}-8\sqrt{3}Q\eta_{(1)}) &= -16k\mu(1+Q)(kb_{t(0)}+\omega b_{x(0)})\\ +6(4+12Q^2+4Q^3-3Q(\omega^2-4))(k^2h_{tt(0)}+2k\omega h_{tx(0)}-\omega^2h_{xx(0)}-\omega^2h_{yy(0)})&\\ -24Q\omega^2k^2h_{yy(0)}-48k^2h_{yy(3)}+\sqrt{3}Q^2(8k^2-3\omega^2)\eta_{(0)}&\end{aligned}\tag{B.2}$$

$$\begin{aligned}\left(k^2-\omega^2\right)(48h_{tt(3)})+8\sqrt{3}Q\eta_{(1)}-48\omega^2h_{yy(3)} &= 16\mu(1+Q)(k^2b_{t(0)}+k\omega b_{x(0)})\\ +6(-4+3(k^2-4)Q-12Q^2-4Q^3)(k^2h_{tt(0)}+2k\omega h_{tx(0)}&\\ +6\omega^2(4(1+Q)^3-3k^2Q)(h_{xx(0)}+h_{yy(0)})+18k^4Qh_{yy(0)}+\sqrt{3}Q^2(3k^2-8\omega^2)\eta_{(0)})&\end{aligned}\tag{B.3}$$

$$\frac{\omega}{k}b_{t(1)}+b_{x(1)}=\mu(1+Q)(\frac{1}{2}(h_{xx(0)}+h_{yy(0)}-h_{tt(0)})-h_{tx(0)})\tag{B.4}$$

$$\frac{3k}{\omega}h_{xy(3)}+3h_{ty(3)}=\mu(1+Q)b_{y(0)}\tag{B.5}$$

Appendix C

Thermo-electric conductivities

Here we show the plots of the thermo-electric conductivities where the results for RN and GR are contrasted. Eq. 5.4 explains why we do not see the effect of the diffusive mode in the longitudinal current since this is suppressed at low ω.

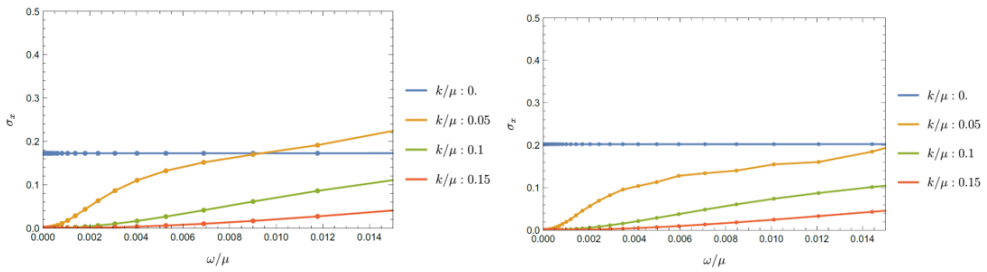

Figure C.1: *Optical conductivities at $T/\mu = 0.1$. left: RN right: GR*

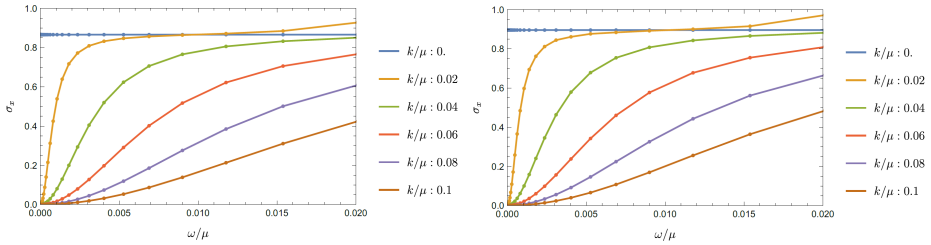

Figure C.2: *Optical conductivities at $T/\mu = 0.5$. left: RN right: GR*

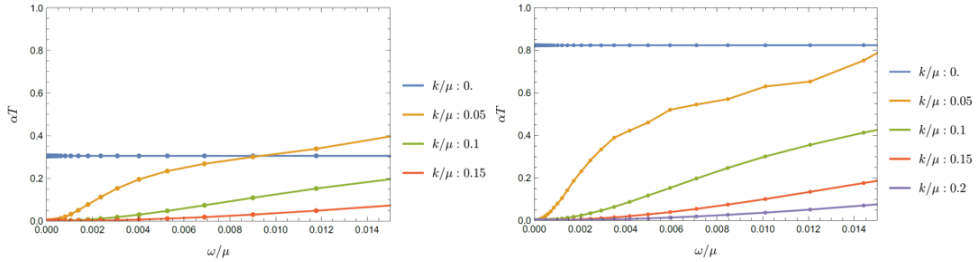

Figure C.3: *Optical thermo-electric conductivities at $T/\mu = 0.1$. left: RN right: GR*

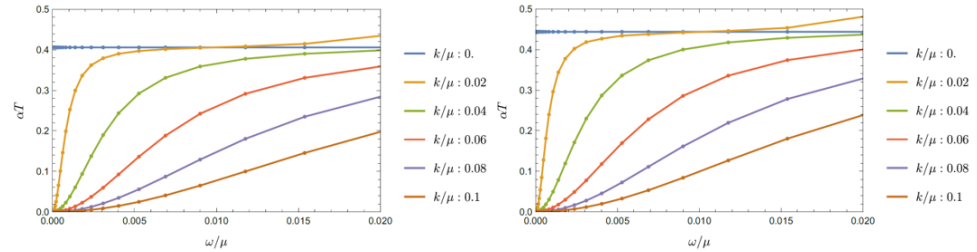

Figure C.4: *Optical thermo-electric conductivities at $T/\mu = 0.5$. left: RN right: GR*

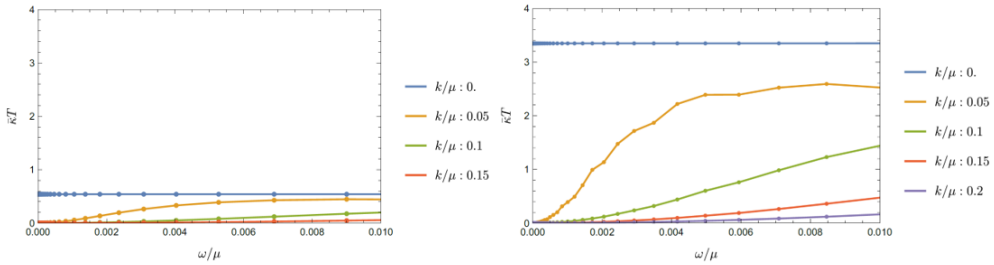

Figure C.5: *Optical thermal conductivities at $T/\mu = 0.1$. left: RN right: GR.*

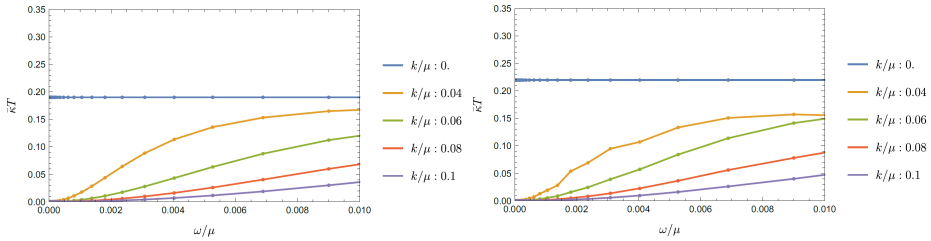

Figure C.6: *Optical thermal conductivities at* $T/\mu = 0.5$. *left: RN right: GR*

Bibliography

[1] J. Maldacena, *The large-N limit of superconformal field theories and supergravity*, International journal of theoretical physics **38**, 1113 (1999).

[2] S. A. Hartnoll, A. Lucas, and S. Sachdev, *Holographic Quantum Matter*, The MIT Press, The MIT Press, Cambridge, 2018.

[3] J. Zaanen, Y. Liu, Y.-W. Sun, and K. Schalm, *Holographic Duality in Condensed Matter Physics*, Cambridge University Press, Cambridge, 2015.

[4] S. S. Gubser, I. R. Klebanov, and A. M. Polyakov, *Gauge theory correlators from non-critical string theory*, Physics Letters B **428**, 105 (1998).

[5] E. Witten, *Anti de Sitter space and holography*, arXiv preprint hep-th/9802150 (1998).

[6] S. Sachdev, *Quantum phase transitions*, Physics world **12**, 33 (1999).

[7] W. Busza, K. Rajagopal, and W. Van Der Schee, *Heavy ion collisions: the big picture, and the big questions*, arXiv preprint arXiv:1802.04801 (2018).

[8] B. Goutéraux and E. Kiritsis, *Generalized holographic quantum criticality at finite density*, Journal of High Energy Physics **2011**, 1 (2011).

[9] S. S. Gubser and F. D. Rocha, *Peculiar properties of a charged dilatonic black hole in AdS 5*, Physical Review D **81**, 046001 (2010).

[10] R. Penrose, *The Road to Reality: A Complete Guide to the Laws of the Universe*, 2007.

[11] J. Zaanen, *Lectures on quantum supreme matter*, 2021.

[12] D. v. d. Marel, H. Molegraaf, J. Zaanen, Z. Nussinov, F. Carbone, A. Damascelli, H. Eisaki, M. Greven, P. Kes, and M. Li, *Quantum critical behaviour in a high-Tc superconductor*, Nature **425**, 271 (2003).

[13] J. Bruin, H. Sakai, R. Perry, and A. Mackenzie, *Similarity of scattering rates in metals showing T-linear resistivity*, Science **339**, 804 (2013).

[14] B. Keimer, S. A. Kivelson, M. R. Norman, S. Uchida, and J. Zaanen, *From quantum matter to high-temperature superconductivity in copper oxides*, Nature **518**, 179 (2015).

[15] J. Zaanen, *Planckian dissipation, minimal viscosity and the transport in cuprate strange metals*, SciPost Physics **6**, 061 (2019).

[16] J. Zaanen, *Why the temperature is high*, Nature **430**, 512 (2004).

[17] G. T. Horowitz, J. E. Santos, and D. Tong, *Optical conductivity with holographic lattices*, Journal of High Energy Physics **2012**, 1 (2012).

[18] A. Donos and J. P. Gauntlett, *Holographic Q-lattices*, Journal of High Energy Physics **2014**, 1 (2014).

[19] M. Baggioli, K.-Y. Kim, L. Li, and W.-J. Li, *Holographic Axion Model: a simple gravitational tool for quantum matter*, Science China Physics, Mechanics & Astronomy **64**, 1 (2021).

[20] S. Arend, *Magneto-Transport of a Reissner-Nordström Holographic Metal*, MSc Thesis, Leiden University (2022).

[21] M. Janse, *Magnetotransport and dissipation in locally quantum critical metals subject to umklapp potentials*, MSc Thesis, Leiden University (2022).

[22] O. Moors, *Drude theory in Reissner-Nordström and Gubser-Rocha holographic strange metals*, MSc Thesis, Leiden University (2022).

[23] J. Post, *DC Transport in Gubser-Rocha Holographic Matter*, MSc Thesis, Leiden University (2022).

[24] F. Balm, *PhD Thesis*.

[25] V. E. Hubeny, S. Minwalla, and M. Rangamani, *The fluid/gravity correspondence*, arXiv preprint arXiv:1107.5780 (2011).

[26] L. P. Kadanoff and P. C. Martin, *Hydrodynamic equations and correlation functions*, Annals of Physics **24**, 419 (1963).

[27] P. Kovtun, *Lectures on hydrodynamic fluctuations in relativistic theories*, Journal of Physics A: Mathematical and Theoretical **45**, 473001 (2012).

[28] R. A. Davison, B. Goutéraux, and S. A. Hartnoll, *Incoherent transport in clean quantum critical metals*, Journal of High Energy Physics **2015**, 1 (2015).

[29] M. Edalati, J. I. Jottar, and R. G. Leigh, *Shear modes, criticality and extremal black holes*, Journal of High Energy Physics **2010**, 1 (2010).

[30] M. Edalati, J. I. Jottar, and R. G. Leigh, *Holography and the sound of criticality*, Journal of High Energy Physics **2010**, 1 (2010).

[31] Y. Ling, C. Niu, J.-P. Wu, and Z.-Y. Xian, *Holographic lattice in Einstein-Maxwell-dilaton gravity*, Journal of High Energy Physics **2013**, 1 (2013).

[32] S. A. Hartnoll, *Lectures on holographic methods for condensed matter physics*, Classical and Quantum Gravity **26**, 224002 (2009).

[33] N. Iqbal and H. Liu, *Universality of the hydrodynamic limit in AdS/CFT and the membrane paradigm*, Phys. Rev. D **79**, 025023 (2009).

[34] B. S. Kim, *Holographic renormalization of Einstein-Maxwell-dilaton theories*, Journal of High Energy Physics **2016**, 1 (2016).

[35] W. R. Inc., *Mathematica, Version 13.0.0*, Champaign, IL, 2021.

[36] A. Krikun, *Numerical Solution of the Boundary Value Problems for Partial Differential Equations. Crash course for holographer*, 2018.